

33

34 **Introduction**

35 Molecular photoswitches are compounds capable to reversibly populate, under the effect of an
36 external perturbation such as the absorption of electromagnetic light, two different stable states,
37 *i.e.* conformation or configuration isomers, that should ideally present significantly different
38 geometries and photochromic properties. The capability of controlling the interconversion
39 between the two states is clearly extremely beneficial in potentially providing molecular-based
40 smart materials or devices, as well as molecular machines converting light energy into
41 mechanical work.

42 Although, their potential is still far from being fully explored, both synthetic and natural
43 photoswitches already found a wide range of applications, including optogenetics and imaging,
44 biotechnology, or pharmacology.

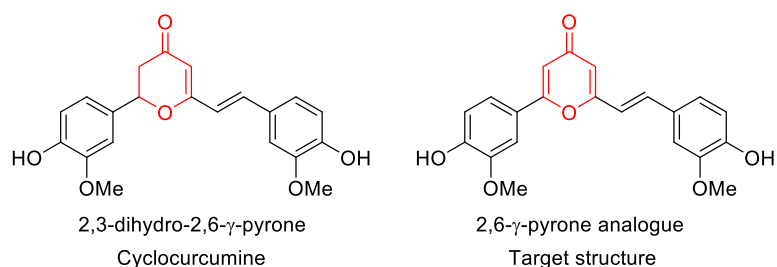
45 The most well-known natural photoswitch is the chromophore of the transmembrane rhodopsin
46 protein, *i.e.* the protonated Schiff-base of the 11-*cis* retinal, which following the absorption of
47 visible light switches into all-*trans* retinal to initiate the cascade leading either to
48 transmembrane ion transport in bacteria or to vision in superior animals. Most notably,
49 rhodopsin-embedded retinal is also one of the most extremely efficient switches both
50 considering the high quantum yield (approaching 80%) and the ultrafast reaction (around 120
51 fs). The molecular and photochemical bases, in terms of the topology of the involved potential
52 energy surfaces (PES) at the base of such efficiency have been deeply characterized by both
53 time-resolved spectroscopy and computational photochemistry,¹ while recently possible dark-
54 photochemistry based isomerization related to photodynamic therapy side effects have also
55 been unraveled.² The combined use of biomimetic strategy and the opportune molecular design
56 is clearly beneficial in improving photoswitching capabilities.³ Several other molecular
57 photoswitches have been reported to date, *i.e.* 9-aryl-phenalenones whose photocyclization is
58 the key step in the defense mechanism of plants against pathogens⁴ or flavylum derivatives,
59 bioinspired from anthocyanins, the natural colorants of most red and blue flowers and fruits.⁵

60 Herein, we report the first bioinspired photoswitch derived from cyclocurcumin (CC). As a
61 matter of fact, CC is a natural compound (Scheme 1), that can be isolated in small amount from
62 turmeric rhizome (*Curcuma longa*). Despite the fact that the remarkable potential
63 pharmacological properties of curcumin are by far driving the most interest, more recent studies
64 revealed the antioxidant, anti-vasoconstrictive, immune-modulating, and neuroprotective
65 effects of cyclocurcumin. However, photoswitching properties of cyclocurcumin were only

66 scarcely investigated, even though they have been demonstrated and rationalized
67 computationally, together with their dependence on the environmental factors.⁶

68 Cyclocurcumin has an α,β -unsaturated dihydropyrone moiety that allows the *trans-cis*
69 photoisomerization of the β ethylenic bound (Scheme 1).⁷ The predominant form of CC both in
70 natural compounds and in solution is the *trans* isomer which is thermodynamically most
71 favorable. Direct *trans-cis* isomerization of CC occurs under irradiation at around $\lambda_{\text{max}} = 375$
72 nm while the reverse reaction takes place thermally or photochemically following the exposure
73 to 300 nm light. CC also exhibits fluorescence emission at around 500 nm, as a function of the
74 solvent. Interestingly, molecular modeling suggests that the competition between the two
75 excited-state relaxation routes, photoisomerization vs fluorescence, is strongly dependent on
76 the polarity of the environment, which ultimately determines the observed outcome.⁶ The
77 competition between the two processes, especially in complex and inhomogeneous biological
78 environments, is detrimental to achieve an exploitable quantum yield. Indeed, an ideal
79 molecular photoswitch should be chemically stable, should have a high photoisomerization
80 yield, large spectral differences between the isomers, and low fatigue, *i.e.* the ability of optical
81 resetting.

82 Furthermore, in order to be exploitable in biological applications and especially in
83 photopharmacology a chromophore should present significant absorption in the biological
84 optical active window, *i.e.* cover the 650 to 1350 nm range in the NIR region. As previously
85 said photoswitching of CC is instead induced by absorption in the UVA region, hence results
86 inapplicable in a biological environment, due to the limited penetration and the possible toxicity
87 of the incident light. One way to circumvent such a limitation resides in exploiting non-linear
88 and in particular two-photon absorption (TPA) properties. Indeed, in this case the simultaneous
89 absorption of two photons having a wavelength of about 740 nm, would be sufficient to
90 populate the isomerizing excited state. Furthermore, TPA probability has a quadratic
91 dependence to the light-source intensity, hence it decays more rapidly when moving away from
92 the incident laser focal point, allowing for a better control of the spatial selectivity that is
93 extremely important in biomedical application, such as photodynamic therapy. While we have
94 shown that natural CC has a relatively high TPA cross-section compared to analogous organic
95 compound, the calculated value of 14 GM is still too low for its veritable exploitation.⁶ For all
96 these reasons, we designed herein an analogue of cyclocurcumin with improved non-linear
97 absorption properties and especially with significantly increased TPA cross-section.



98

99

Scheme 1. Natural cyclocurcumin and its 2,6- γ -pyrone analogue

100

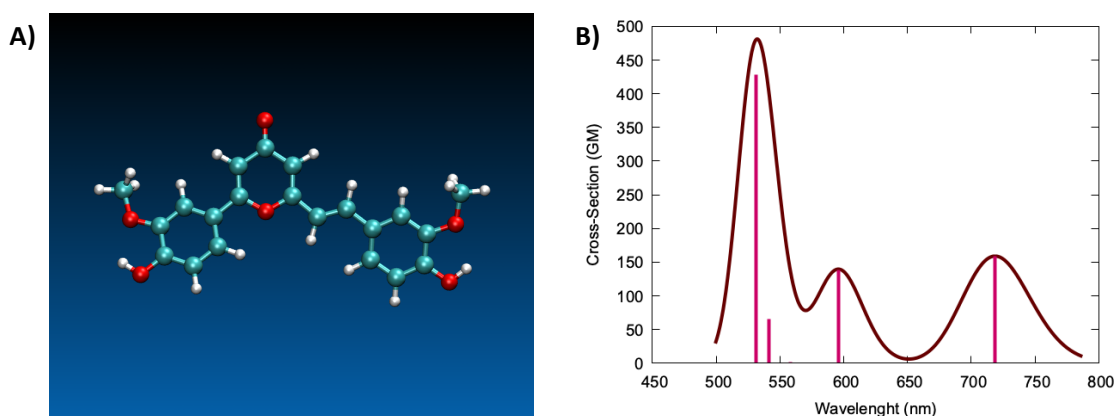
101 We thus propose a 2,6- γ -pyrone analogue (Scheme 1) with an additional ethylene bond
 102 compared to the 2,3-dihydro-2,6- γ -pyrone core of CC to i) increase the planarity of the structure
 103 and to ii) introduce a second donor-acceptor group (aryl-ketone) increasing molecular
 104 symmetry. Indeed, planar and quadrupolar structures D- π -A- π -D, such as the one of pyrone,
 105 are expected to be more efficient in TPA than their dipolar analogues D- π -A, such as
 106 cyclocurcumin.⁸

107 **Results and discussion**

108 **1. Equilibrium geometry**

109 TPA cross-section efficiency in organic compounds can be easily related to their molecular
 110 structures. TPA efficiency is founded on a rather complex theory, developed by Maria Göppert-
 111 Mayer in 1931, and based on the presence of intermediate fictive states allowing to overcome
 112 the formally quantum-physically prohibited simultaneous absorption of two-photons. However,
 113 practical rules of the thumb relating TPA efficiency and the specific molecular architecture
 114 exist and can be used. In particular, it can be shown that planar and centrosymmetric
 115 arrangements are extremely beneficial to increase TPA cross-section. Analogously, the
 116 presence of charge-transfer excited states can also be pointed out for its most favorable
 117 influence. More specifically, quadrupolar molecules presenting an alternance of donor (D) and
 118 acceptor (A) units linked by conjugated bridges (π), *i.e.* D- π -A- π -D structures are most
 119 favorable molecular scaffolds to achieve high and exploitable cross-section and are more
 120 efficient than their dipolar analogues D- π -A, such as CC.⁸ When examining the molecular
 121 formula and the equilibrium geometry of cyclocurcumin, the breaking of the planarity induced
 122 by the free rotation of the phenyl group in position 2 can be seen as a further reason of the
 123 simulated moderate cross-section for the natural occurring compound. To fix the planarity issue,
 124 a most promising possibility could be to introduce a double bond leading to a pyrone core.

125 Indeed, the optimization of the geometry of the thermodynamically favored E-isomer of 2,6- γ -
126 pyrone, performed at density functional (DFT) level of theory, has shown the quasi-planarity
127 of the organic core (Figure 1) as also quantified by the dihedral angle between the phenyl ring
128 and the pyrone moiety that reaches the value of 160° in contrast to the almost perpendicular
129 arrangement observed for natural CC.



130

131 **Figure 1.** Equilibrium ground-state geometry simulated at DFT level (A) and TPA absorption
132 spectrum (B) of our targeted 2,6- γ -pyrone **22** calculated at CAM-B3LYP level of theory. Note
133 that the absorption spectrum has been obtained by convoluting the vertical transitions,
134 represented as vertical sticks, with gaussian functions of fixed width at half-length of 0.3 eV.

135

136 The influence of the oxidation on the linear optical properties of our targeted compound, as
137 obtained by state-of-the-art molecular modeling, will be discussed in the following. Here, and
138 to justify the forthcoming synthetic efforts, we only report simulated TPA spectrum in water
139 that would be the most relevant solvent for biological applications. Note that, as detailed in
140 Section 3.1, CAM-B3LYP functional is the one better reproducing the optical properties of our
141 compound, and hence was retained for modeling TPA. As can be seen from Figure 1, the
142 simulated TPA previews that the non-linear absorption to the S_1 (π - π^*) state will take place in
143 the NIR, with a maximum at 719 nm. Notably, the corresponding band is well separated from
144 the one leading to the S_2 (n - π^*) absorption and most importantly is characterized by a cross-
145 section of 159 GM. This value represents an order of magnitude increase in the TPA
146 performance over the parent CC, which peaked at only 14 GM in the NIR range.⁶ This could
147 be also assigned to the enhancement of planarity of the scaffold that leads to a quadrupolar
148 arrangement of D- π -A- π -D type. Remarkably, absorption to the S_2 state also led to a band

149 whose tails would partially cover the biological active window, peaking at around 600 nm and
150 having cross-section of 139 GM. Absorption to higher excited states leads to band appearing in
151 the visible part of the spectrum, and hence being less exploitable despite their high cross section.

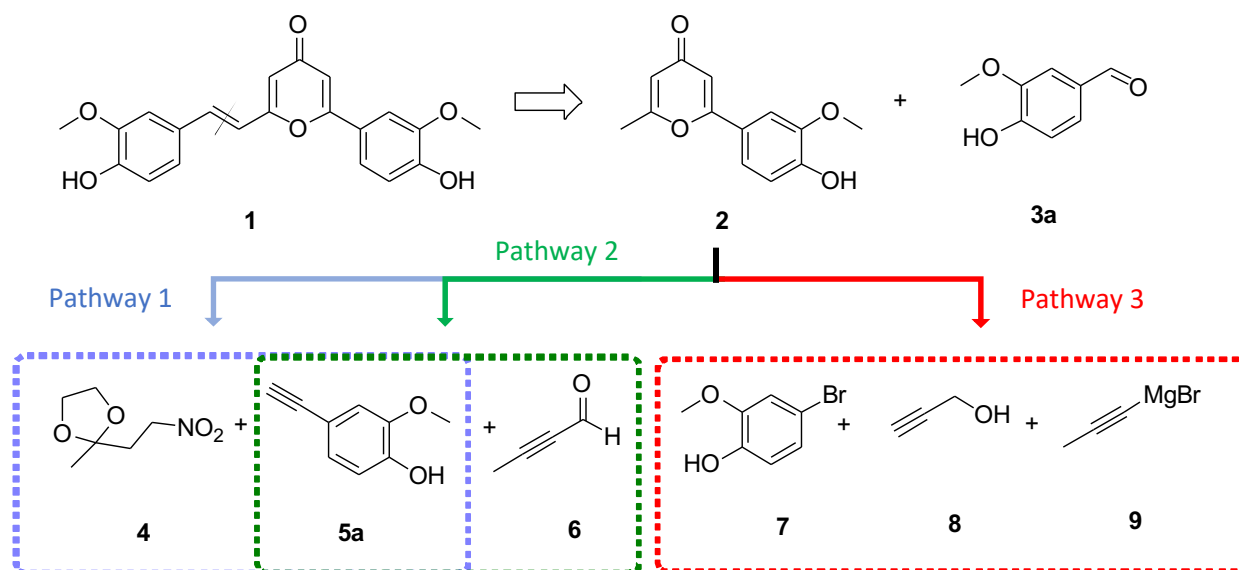
152 Globally, the results of molecular modeling are consistent in previewing a considerable increase
153 of the optical properties of the target biomimetic analogous, thus justifying the efforts in
154 synthetic methodology that have been undertaken and that are presented in the following
155 section.

156

157 **2. Synthesis of 2,6- γ -pyrone analogue of cyclocurcumin**

158 The retrosynthetic pathway proposed herein for the synthesis of targeted 2,6- γ -pyrone
159 analogue of cyclocurcumin is given in Scheme 2. This consists in the aldolization/crotonization
160 reaction of an alkylated vanillin and the methyl group of 2,6- γ -pyrone **1** and leading to a
161 photoisomerizable carbon-carbon double bond.

162 Our strategy was based on the formation of the γ -pyrone ring, the di-dehydrogenated
163 equivalent of the 2,4-dihydro- γ -pyrone ring, present in cyclocurcumin. Various synthetic routes
164 affording to symmetrically or asymmetrically in 2,6 positions were already described in the
165 literature according to classical methods such as: (i) the cyclocondensation of the dienol of
166 1,3,5-tricarbonyl compounds under mild acidic catalysis (*i.e.* Brønsted acids such as triflic acid
167 or *p*-toluenesulfonic acid),^{9,10} (ii) the cyclization of diynone,^{11,12,13} or *via* an original pathway
168 using an isoxazole intermediate.¹⁴ Herein, we chose to implement the strategies involving either
169 a diynone intermediate, as the most explored and documented pathway to form a γ -pyrone ring,
170 and the one involving an oxazole intermediate *a priori* faster and offering good yields. Thus,
171 three synthetic ways were evaluated for the formation of the central pyrone moiety, namely (i)
172 with nitro and terminal alkyne fragments **4** and **5a** (pathway 1, Scheme 2), (ii) alkyne **5a** and
173 butynal **6** (pathway 2, Scheme 2) or (iii) bromoguaiacol **7**, propargyl alcohol **8** and 1-
174 propynylmagnesium bromide **9** (pathway 3, Scheme 2).



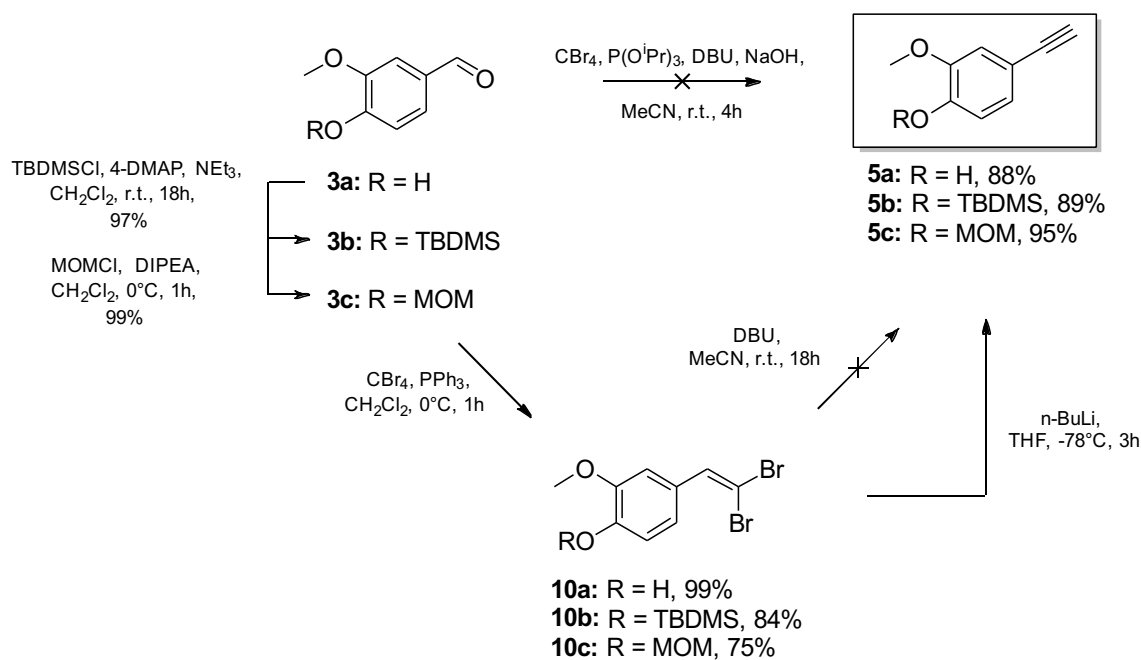
175

176 **Scheme 2.** Retrosynthetic pathways for the formation of dissymmetric 2,6- γ -pyrone **1**

177

178 In the first pathway, the synthesis of **2** was envisaged through the synthesis of isoxazole
 179 intermediate **11**, which is previously generated from the two building blocks **4** and **5a** (Scheme
 180 2, Pathway 1). This procedure is similar to the one previously reported by Li *et al.* and it is
 181 based on the 1,3-dipolar cycloaddition reaction between the acetylene **5a** and the nitrile oxide,
 182 generated *in situ* from fragment **4**.¹⁴ According to the authors, the presence of the 2-oxoalkyl
 183 chain in position 3 of isoxazole should allow, after reduction by Mo(CO)₆ to an enamino ketone
 184 intermediate, which is cyclized under acidic conditions into the corresponding γ -pyrone **2**.

185 The general reaction scheme corresponding to the first retrosynthetic pathway is given in
 186 Schemes 3 and 4. Compounds **5a-c** (Scheme 3) could have been obtained one pot by
 187 transforming the aldehyde group of vanillin derivatives (**3a-c**) into a terminal alkyne as
 188 proposed by Doddi and coll.¹⁵ This implies the use of modified Ramirez olefination^{16,17} (CBr₄
 189 and triisopropyl phosphite P(OⁱPr)₃ to avoid the elimination of triphenylphosphine oxides)
 190 followed by modified Corey-Fuchs reaction using the 1,8-diazabicyclo[5.4.0]undec-7-ene
 191 (DBU) and NaOH as base. Unfortunately, terminal alkynes **3a-c** could not be obtained
 192 according to this method. Thus, the synthesis was done in two-steps involving i) a Ramirez
 193 olefination of aldehyde to give 1,1'-dibromoalkenes **10a-c** in good yields then ii) Corey-Fuchs
 194 reaction (Scheme 3).^{18,19} For this latest way, the reaction performed with DBU only led to very
 195 low yields (< 10%).²⁰ Finally, the classical Corey-Fuchs reaction carried out with *n*-BuLi as
 196 base at -78°C gave the desired terminal alkynes **5a-c** with an excellent yield (Scheme 3).



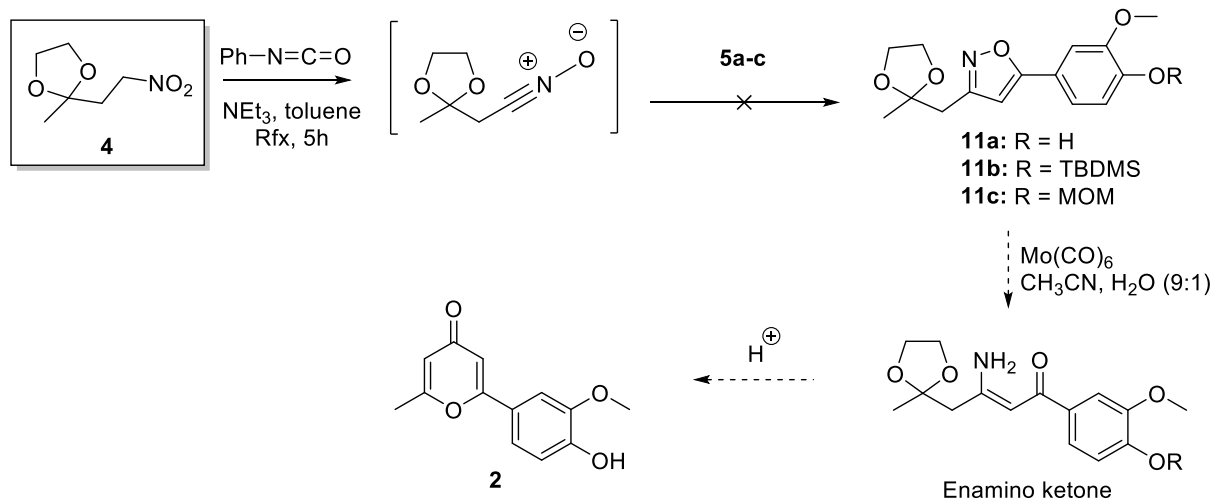
197

198

199

Scheme 3. Synthetic pathway to obtain terminal alkyne **5**.

200 In parallel, the synthon **4** was prepared, according to the literature, from methyl vinyl ketone
 201 and sodium nitrite in acidic conditions followed by carbonyl protection as dioxolane.^{21,22}
 202 However, in our experiments, the two reaction steps afforded to yields lower than 30% as well
 203 as to the formation of the 1,4-adduct of the acetate on the conjugated carbonyl as main product.
 204 Then, the conversion of the **4** into the corresponding nitrile oxide precursor was tested *in situ*
 205 under Mukaiyama's dehydration conditions using phenyl isocyanate.²³ Unfortunately, the
 206 expected heterocyclic compounds **11a-c** could not be isolated, probably due to the instability
 207 of the nitro derivative **4** or the non-formation *in situ* of the nitrile oxide intermediate (Scheme
 208 4). Therefore, this strategy was not further explored.



209

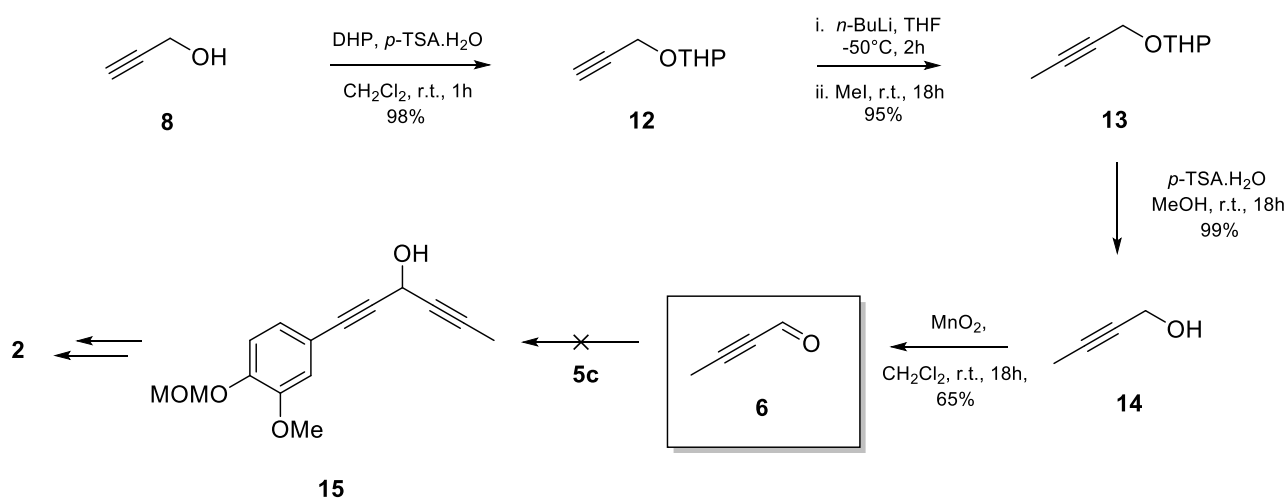
210

Scheme 4. First strategy considered to obtain the 2-aryl- γ -pyrone **2**

211

212 The second pathway envisaged to form γ -pyrone **2** was based on the internal cyclization
 213 of a diynone (Scheme 2, Pathway 2). In this second strategy the targeted intermediate was
 214 diynol **15**, which could be potentially synthesized from aldehyde **6** and the alkyne **5c** (Scheme
 215 5), then oxidized in ketone and cyclized into **2**.

216



218

Scheme 5. Bottom-up approach to obtain the 2-aryl- γ -pyrone **2**.

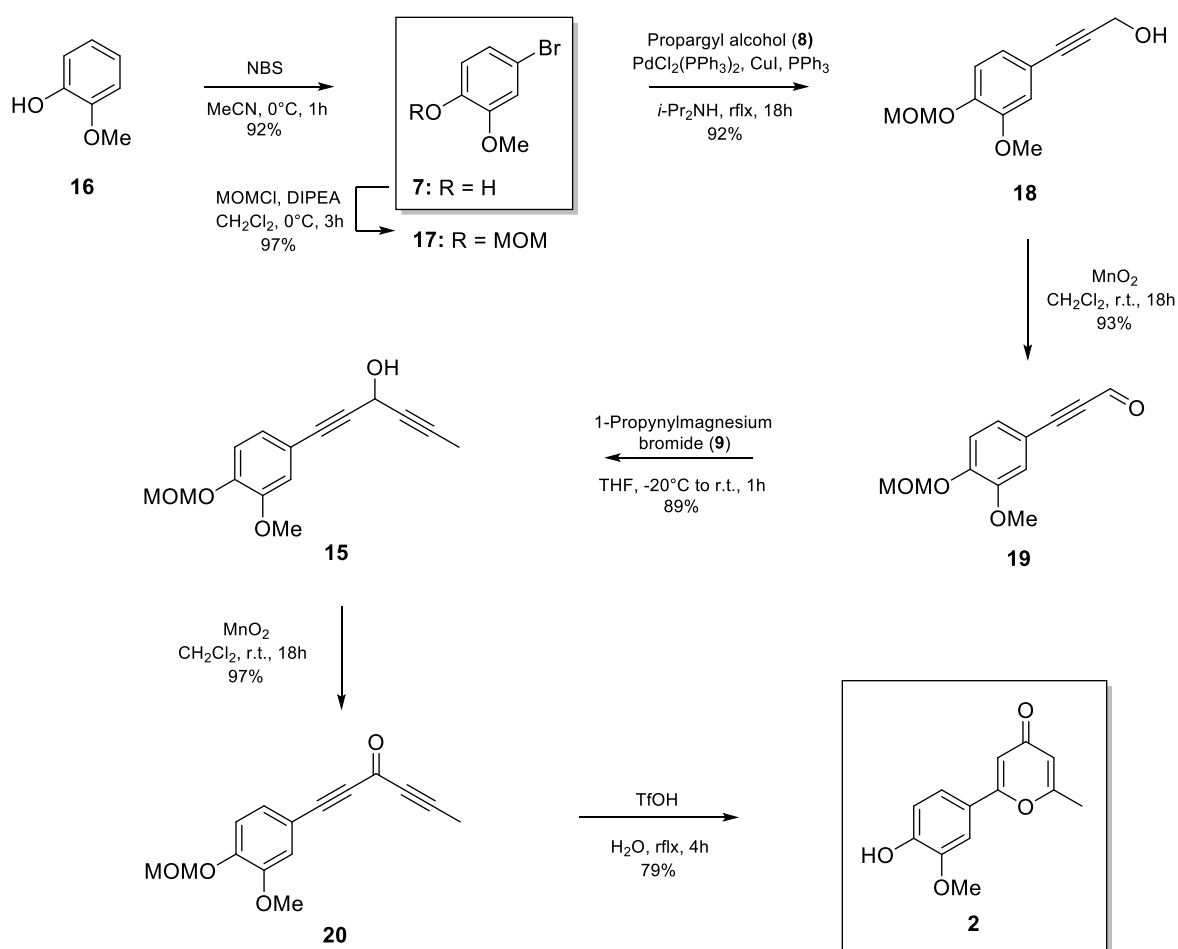
219

220 In this bottom-up approach, the commercial propargyl alcohol (**8**) was easily protected as
 221 tetrahydropyranyl ether, compound **12**, with dihydropyrane (DHP) in CH_2Cl_2 and acidic
 222 media.^{24,25} The terminal alkyne was then alkylated with methyl iodide and *n*-BuLi (Scheme 5,
 223 compound **13**), and deprotected in the presence of *p*-TSA to give the expected 2-butynyl alcohol
 224 **14**.²⁶ The last was oxidized with an excess of MnO_2 to afford the corresponding 2-butynyl
 225 aldehyde **6**.²⁷ This aldehyde should have been coupled with terminal alkyne fragment protected
 226 terminal alkyne **5c** to give the diynol derivative **15**.^{28,29} Unfortunately, in addition to partial
 227 polymerization (described as inevitable in the literature), the aldehyde **6** got oxidized into the
 228 corresponding carboxylic acid, and thus despite our various precautions (low temperature, dry
 229 and free oxygen conditions).³⁰ Thus, this strategy was not suitable for further developments.

230 Finally, the diynol **15** was synthesized from guaiacol (**16**) according to the third retrosynthetic
 231 pathway (Scheme 2) *via* a top-down approach. After a regioselective bromination with NBS
 232 (Scheme 6, compound **7**) and protection of phenolic function, the MOM protected

233 bromoguaiacol was obtained with an overall yield of 90% (Scheme 6, compound **17**).^{31,32,33}
 234 Then, a Sonogashira coupling using propargyl alcohol (**8**) in the presence of palladium complex
 235 catalyst as well as copper co-catalyst led to butynyl alcohol derivative **18** in good yield.³⁴ The
 236 oxidation with an excess of manganese dioxide gave aldehyde **19** which did not exhibit the
 237 instability of **6**.^{27,35} The ynone **19** could undergo the addition of 1-propynylmagnesium bromide
 238 (**9**) to give the expected aryl-hexa-1,4-diyne-3-ol **15** with a yield of 89%.¹¹ The last step before
 239 the cyclization in γ -pyrone was the oxidation of **15** in corresponding ketone **20** using MnO_2 .^{11,36}
 240 Thus, according to this synthetic way the γ -pyrone's precursor **20** was obtained with an overall
 241 yield of 66%. Then, the cyclization of diyne **20** was performed *via* acid-mediated reaction
 242 (with triflic acid) in the presence of water, as previously described.³⁷ The target 2-aryl- γ -pyrone
 243 **2** was obtained with a good yield (52% in 7 steps) and was fully characterized by NMR, mass
 244 spectrometry and elemental analysis.

245



246

247

248

Scheme 6. Top-down approach leading to γ -pyrone core **2**.

249 To optimize the conditions of the aldolization/crotonization reaction between compounds **21**
250 (MOM-protected γ -pyrone core) and **3c**, various parameters have been investigated, *i.e.* the
251 nature and quantity of base, reaction time and temperature (Scheme 7 and Table 1).^{38,39}

252

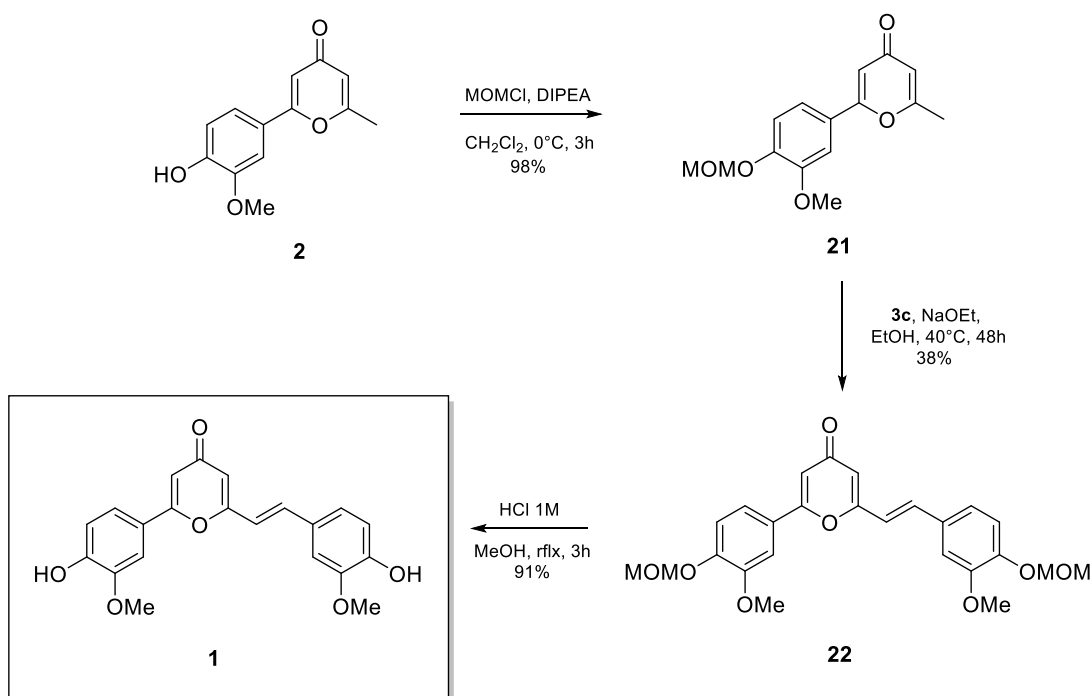
253 **Table 1.** Influence of the base, time, and temperature on the reaction yield and stereoselectivity
254 between compounds **21** and **3c**.

Entry	Base	Time (h)	T (°C)	Yield (%)	<i>E/Z</i> molar ratio
1	NaOMe (1.2 eq)	18	25	Traces	n.d.
2	KOH (1.2 eq)	18	25	21 degradation	n.d.
3	NaOEt (1.2 eq)	18	25	20	1/1
4	NaOEt (1.2 eq)	48	40	38	95/5

255

256 On one side, only traces of the expected alkene were obtained with solid sodium methanolate
257 or potassium hydroxide, the latest even inducing the degradation of the pyrone cycle. On the
258 other side, the expected alkene was formed in moderate yield with freshly prepared sodium
259 ethanolate. However, when the reaction was carried out at 25°C for 18 h, the product was
260 isolated with only 20% yield and showed no stereoselectivity. An increase of the temperature
261 to 40°C and reaction time to 48h was necessary to improve the conversion and to isolate after
262 chromatography the product with 38% yield. In those conditions, an enhancement of
263 stereoselectivity was observed, isomer *E* being the major stereoisomer.

264 The optimized conditions (Table 1, line 4) were then used to couple the protected aryl- γ -pyrone
265 **21** (Scheme 7) with MOM-protected vanillin **3c**. The desired compound **22** was obtained with
266 38% yield. A final acidic deprotection of aryl- γ -pyrone moieties afforded quasi-quantitatively
267 the target derivative **1**, analogue of cyclocurcumin.⁴⁰ This newly reported compound was fully
268 characterized by NMR and HRMS which confirmed the molecular structure.



269

270 **Scheme 7.** Synthetic pathway leading to **1**, 2,6- γ -pyrone analogue of cyclocurcumin.

271

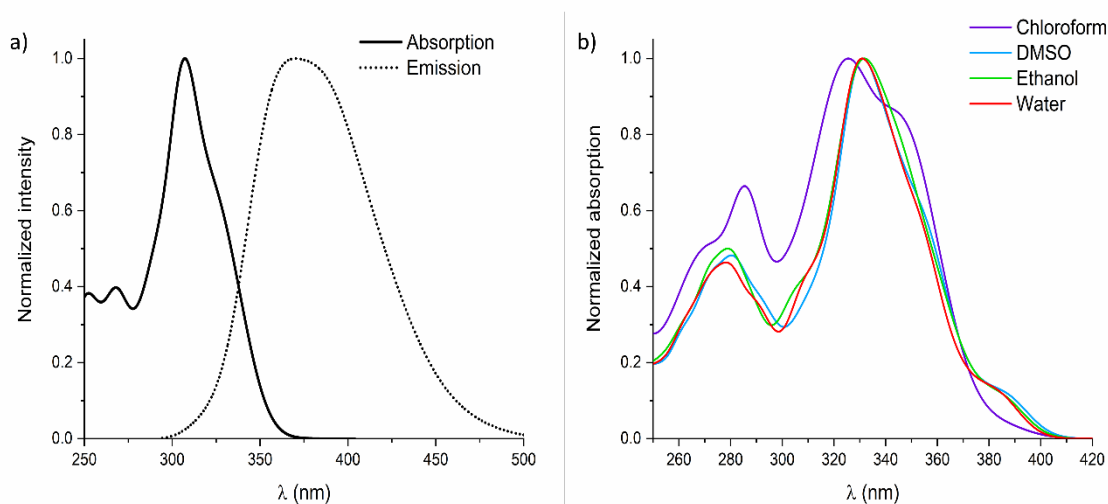
272 **3. Photophysical properties of 2,6- γ -pyrone analogue of cyclocurcumin, **1****

273 **3.1. Simulated absorption and emission spectra.**

274 One-photon absorption spectrum was computed for comparison with experiment. To that
 275 purpose, different DFT functionals and basis sets were benchmarked to characterize the
 276 excitation of the molecule, see in the ESI for more details.

277 CAM-B3LYP functional gave the best representation of the excited state manifold as compared
 278 to the other functional. This agreement holds despite a considerable shift in the absolute value
 279 of the absorption wavelengths that is common for range-separate functionals. It can be related
 280 to an improved representation of charge-transfer states compared to hybrid functionals that
 281 avoids the presence of significant intruder states, whose excitation energy would have been
 282 artificially lowered. In Figure 2, the calculated absorption spectrum is shown taking into
 283 account the vibrational and dynamic effects modeled *via* a Wigner distribution sampling around
 284 the stationary minimum. Also, the emission spectrum was calculated sampling the most stable
 285 minimum in the excited state in the gas phase. In the case of the absorption spectrum *in vacuo*
 286 we observe an absorption maximum at around 310 nm, while the emission spectrum is
 287 considerably stoked-shifted peaking at 375 nm. Note also the important asymmetry of the
 288 absorption band due to the vibronic coupling and the large and rather shoulderless emission

289 band. Both absorption and emission spectra match reasonably with the experimental ones,
290 reported in the next section.



291

292 **Figure 2.** Absorption and emission spectra in the gas phase of 2,6- γ -pyrone analogue at the
293 CAM-B3LYP level (left). Absorption spectra in different solvents using PCM (right).

294

295 In conjunction with the gas phase exploration of the absorption and emissive properties,
296 solvatochromism was investigated including the solvent effects implicitly via a dielectric
297 medium in the polarizable continuum model (PCM) approach (Figure 2 right). A slight red shift
298 of the absorption maximum was observed when increasing the polarity of the solvent. Most
299 remarkably, the spectrum in chloroform presents a noticeable shoulder at a wavelength higher
300 than λ_{max} . The appearance of this feature might be due to a complex coupling between the
301 electronic and nuclear degrees of freedom and most notably to the mixing of the lowest lying
302 ($n-\pi^*$) and ($\pi-\pi^*$) states that is strongly dependent on the specific sampled geometry.

303

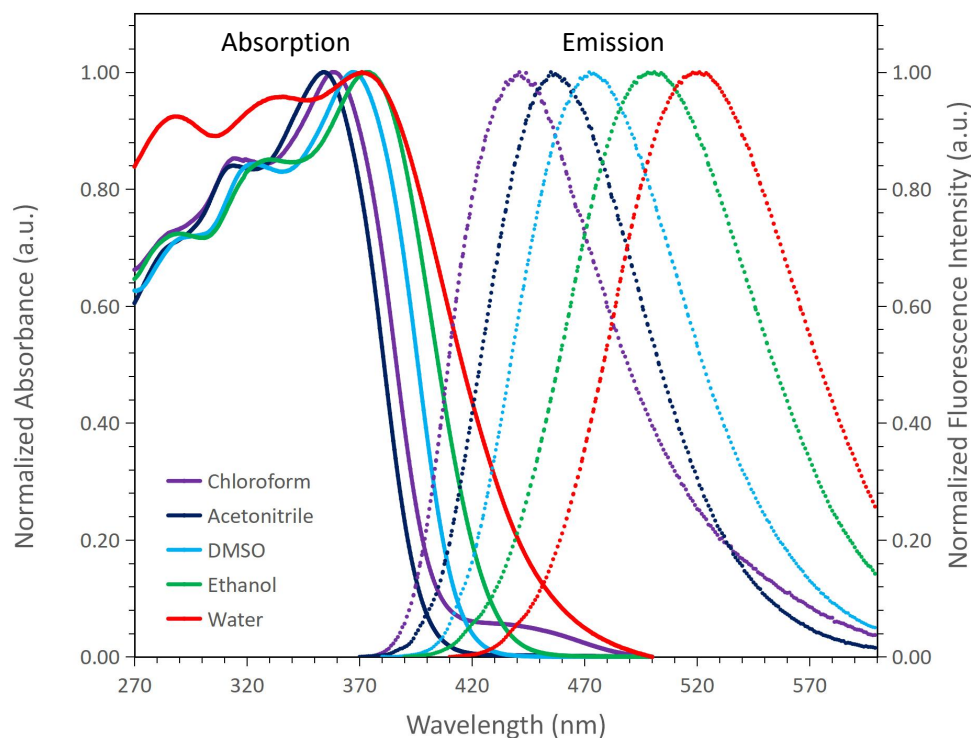
304 3.2. Experimental absorption and emission spectra.

305 The photochromic properties of the 2,6- γ -pyrone analogue of cyclocurcumin, **1**, were
306 investigated in aprotic and protic solvents with various polarities (*i.e.* CHCl_3 , MeCN, DMSO,
307 EtOH and H_2O). The steady-state absorption spectra of the pyrone at the ground state are shown
308 in Figure 3 and correspond mainly to the *E*-isomer as determined from NMR (Figure 5) (*E/Z*
309 ratio of 100:0 in DMSO and 92:8 in EtOH). All spectra exhibit three broad absorption peaks,

310 centered on ~ 288 , 327 and 374 nm in ethanol. The highest and the lowest energy absorption
311 band were assigned to be mainly due to the $\pi-\pi^*$ transition of the phenyl-pyrone moiety (D₁-
312 π -A) and the styryl-pyrone moiety (A- π -D₂), respectively (Figure 3), while the intermediate
313 energy absorption band was assigned to the $n-\pi^*$ transition. The values related to the styryl-
314 pyrone moiety are similar to the ones reported for cyclocurcumin, which exhibit in ethanol a
315 main absorption peak at ~ 370 nm and a shoulder at ~ 330 nm.³ This is consistent with the fact
316 that the additional double bond in the pyran cycle is not inducing any extension of π -conjugation
317 on the styryl-pyrone moiety (A- π -D₂), but rather an extension of planarity from one extreme to
318 the other of the molecule (Figure 1).

319 An overall positive solvatochromism is observed which corresponds to a bathochromic shift (or
320 red shift) with increasing solvent polarity. This could be due to a more important stabilization
321 of the bright state ($\pi-\pi^*$) due to the higher dipolar moment of this excited state. The molar
322 extinction coefficients (Table 2) at the respective maxima band are also depending on the
323 solvent, the highest value being obtained in MeCN ($31654 \text{ M}^{-1} \text{ cm}^{-1}$) and the lowest in H₂O
324 ($14632 \text{ M}^{-1} \text{ cm}^{-1}$).

325 The fluorescence spectra of 2,6- γ -pyrone analogue of cyclocurcumin were obtained upon
326 excitation at the maxima band and are given in Figure 3. Whatever the solvent, a broad
327 fluorescence spectrum is observed which maximum is Stokes shifted and is increasing with
328 increasing solvent polarity. This indicates that the excited-state dipole moment of the pyrone is
329 significantly larger than that of its ground state. Whatever the solvent, the quantum yields of
330 fluorescence (ϕ) are low and do not exceed 2% (see Table 2). The lowest and the highest ϕ of
331 2,6- γ -pyrone were of 2% in DMSO and less than 1% in water, respectively. Those values are
332 much lower than the one of cyclocurcumin which has a fluorescence quantum yield of 9% in
333 chloroform (*vs* 1.5% for the pyrone analogue) and of 3% in acetonitrile (*vs* 1.3% for the pyrone
334 analogue).³



335

336 **Figure 3.** Normalized absorption (left) and emission (right) spectra of 2,6- γ -pyrone **1** upon
 337 excitation at λ_{max} in chloroform, acetonitrile, DMSO, ethanol and water.

338 **Table 2.** Optical properties of 2,6- γ -pyrone **1** and kinetics of the photoisomerization process.

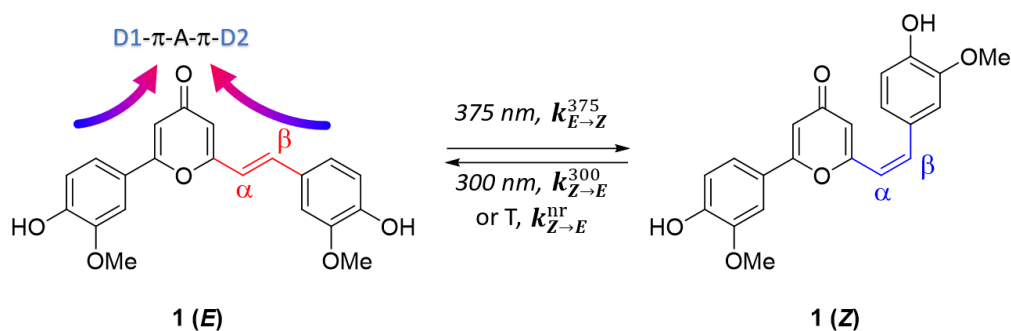
	CHCl ₃	CH ₃ CN	DMSO	EtOH	H ₂ O
λ_{abs} (nm)	358	354	367	374	371
ϵ_{B} (M ⁻¹ cm ⁻¹)	27000	31654	27927	27220	14632
λ_{em} (nm)	441	455	472	501	516
ϕ_{F} (%)	1.5	1.3	2.0	1.8	<1
<i>E/Z</i> (GS)*	n.d.	n.d.	100/0	92/8	n.d.
<i>E/Z</i> (PSS)*	n.d.	n.d.	47/53	25/75	n.d.
<i>E</i> → <i>Z</i> at 25°C, 375 nm**					
$k_{E \rightarrow Z}^{375} \cdot 10^3$ (s ⁻¹)	30	18	12	16	n.d.
$t_{1/2}^{375}$ (s)	23	39	58	43	n.d.
<i>Z</i> → <i>E</i> at 25°C, 300 nm**					
$k_{Z \rightarrow E}^{300} \cdot 10^3$ (s ⁻¹)	127	124	182	145	n.d.
$t_{1/2}^{300}$ (s)	5.5	5.6	3.8	4.8	n.d.
<i>Z</i> → <i>E</i> non-radiative (nr)**					
$k_{Z \rightarrow E}^{\text{nr}} \cdot 10^6$ (s ⁻¹) at 25°C**	1.6	<1	<1	4.4	n.d.
$t_{1/2}^{\text{nr}}$ (h) at 25°C	120	>168	>168	44	n.d.
$k_{Z \rightarrow E}^{\text{nr}} \cdot 10^6$ (s ⁻¹) at 40°C**	38.9	2.7	14.7	5.3	n.d.
$t_{1/2}^{\text{nr}}$ (h) at 40°C	5.0	71	13	36	n.d.

339 * as determined from NMR measurements.

340 ** as determined from UV-VIS measurements.

341

342 The decrease in the fluorescence of 2,6- γ -pyrone **1** compared with cyclocurcumin could be
343 attributed to the enhancement of nonradiative decay processes such as the excited-state
344 isomerization of the styryl double bond. Moreover, this nonradiative deactivation process
345 should be favored by the decrease of internal conversion of pyrone, more rigid and more planar
346 than cyclocurcumin that can adopt several rotamers conformations. To further investigate this
347 hypothesis, we characterize the photoisomerization process (Scheme 8) through combined
348 steady-state absorption and NMR experiments.



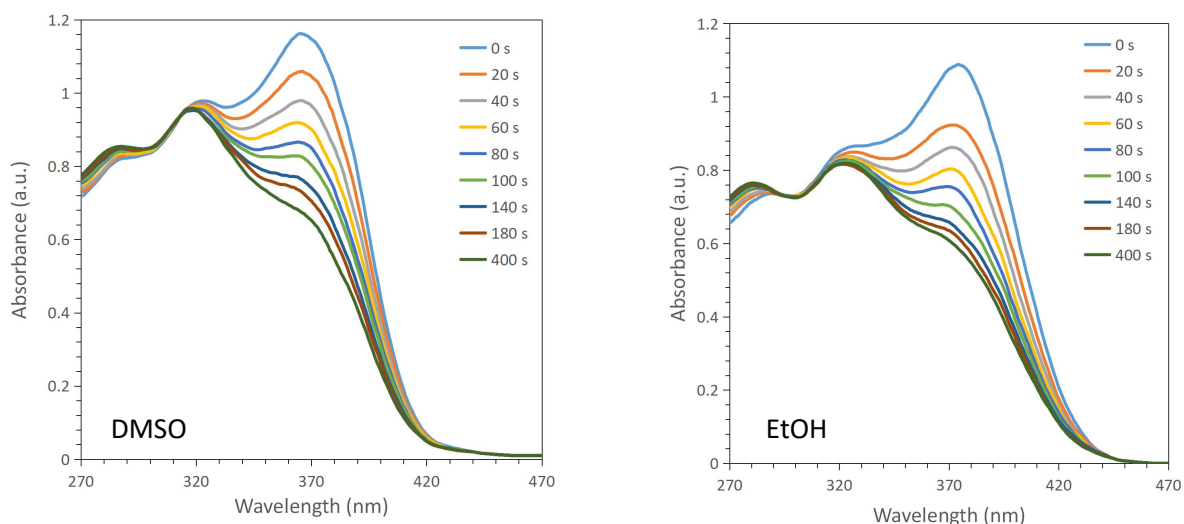
349

350 **Scheme 8.** Reversible *E/Z* photoisomerization scheme of the quadrupolar compound **1**
351 showing direct isomerization upon irradiation at 375 nm and reverse reaction taking place
352 either by irradiation at 300 nm or thermally, in the dark

353

354 3.3. Characterization of the photoisomerization efficiency.

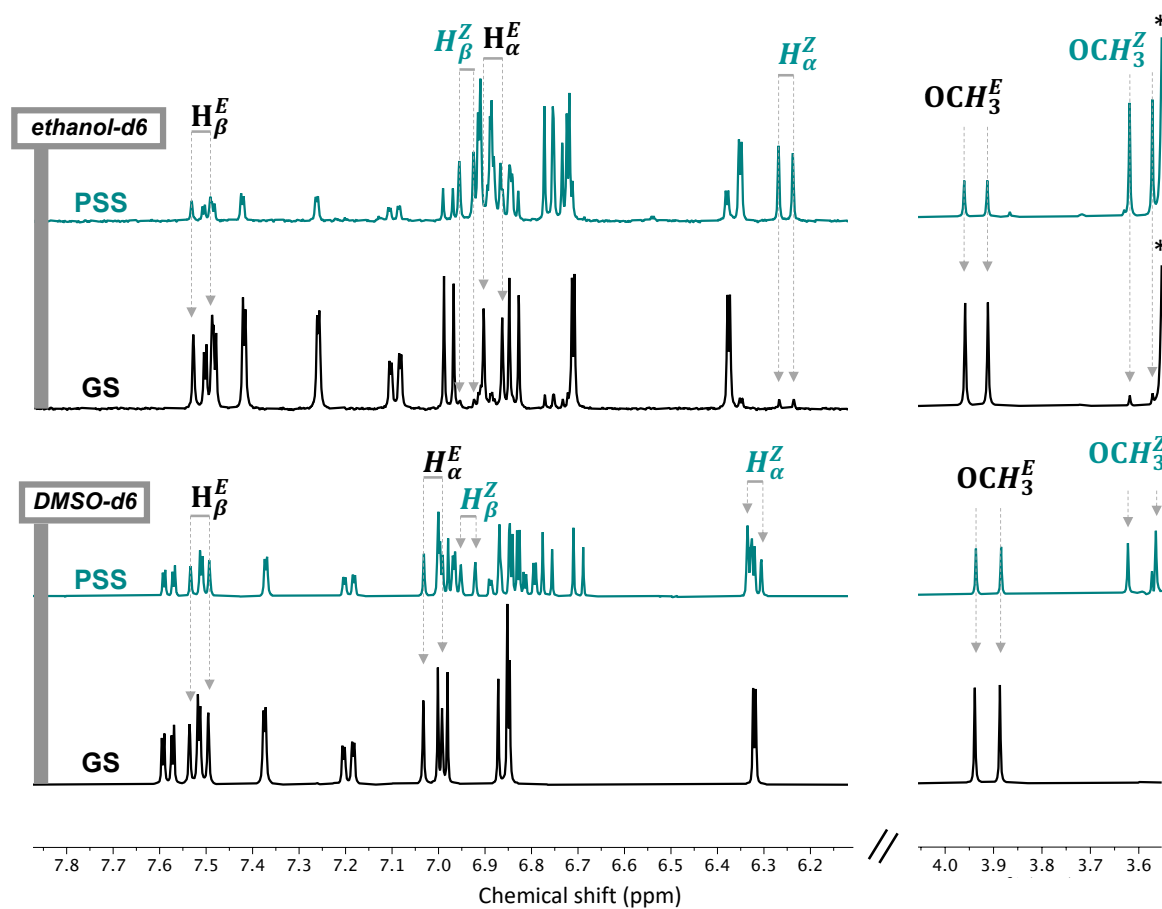
355 The isomerization of 2,6- γ -pyrone is a reversible process in which (i) the direct isomerization
356 consists in the photo-induced transformation of *E* into *Z*-isomer upon irradiation at a
357 wavelength close to the λ_{\max} of the *E*-isomer. The back-switch represents the reverse reaction
358 that takes place either by irradiation at 300 nm or thermally, in the dark (Scheme 8). This
359 process can be followed either by monitoring the time-evolution of the UV/Vis absorption
360 spectrum and in particular of the intensity of the signature 370 and 300 nm bands (Figure 4), or
361 the modification in the chemical shifts on the ^1H NMR spectra (Figure 5).



362

363 **Figure 4.** Spectral evolution the $E \rightarrow Z$ photoisomerization from the ground state to the
 364 photostationary state, upon irradiation at 375 nm in DMSO (left) and in ethanol (right)

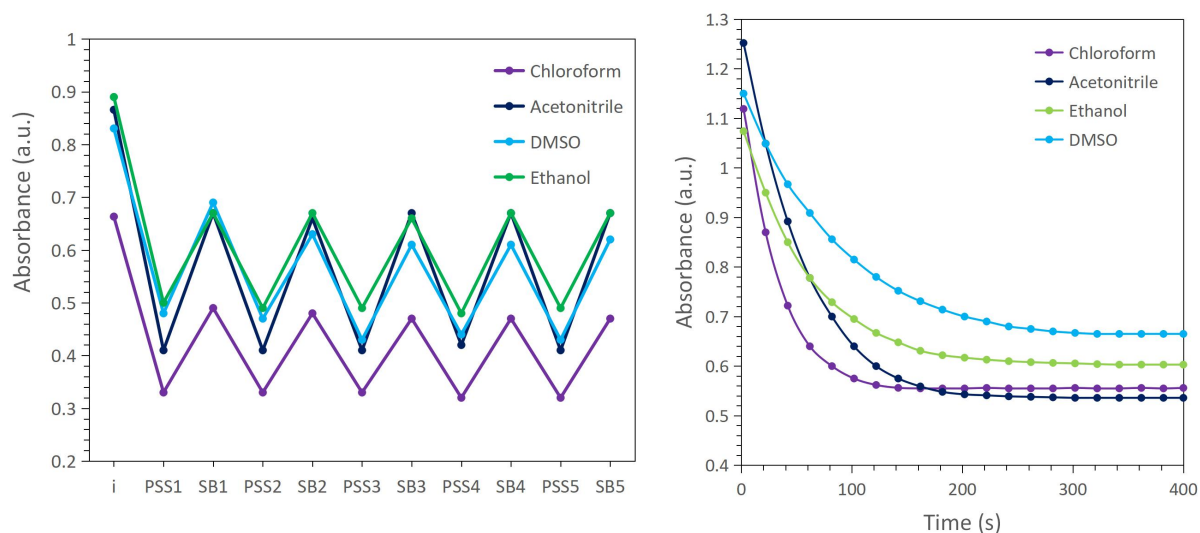
365



366

367 **Figure 5.** Representative ^1H NMR spectra of the 2,6- γ -pyrone **1** in ethanol- d_6 and DMSO- d_6
 368 at both ground state (black line) and photostationary state (cyan line).

370 At first, NMR experiments were performed to characterize both the ground state (GS) and the
371 photostationary state (PSS). Full NMR spectra and peak positions of 2,6- γ -pyrone are provided
372 in Supporting Information. While *E*-form is the thermodynamically favored isomer, the
373 interconversion into *Z* can be induced upon irradiation at a wavelength close to the maximum
374 absorption band, of about 370 nm. Figure 5 shows the most important changes in the ^1H NMR
375 spectrum observed between the GS and the PSS, in ethanol-*d*₆ and DMSO-*d*₆. For instance, in
376 DMSO, the protons of the *E*-form of styryl moiety were assigned at 7.52 (H_β^E) and 7.01 (H_α^E)
377 and the one of the *Z*-form at 6.94 (H_β^Z) and 6.32 ppm (H_α^Z). Those protons can be easily
378 identified since the vicinal coupling constants are always larger for *E* ($J_{\text{HH}} = 12\text{-}18$ Hz, herein:
379 16.1 Hz) than for *Z*-isomers ($J_{\text{HH}} = 0\text{-}12$ Hz, herein: 12.1 Hz). As a general trend, the intensity
380 of the protons of the *E* styryl moiety is decreasing upon excitation at 375 nm. However, they
381 appear within a multiplet and therefore the accurate quantification of the *E/Z* ratio, via the peak
382 integrals is rather cumbersome. Hence, we instead quantified the protons belonging to the two
383 -OCH₃ groups appearing at 3.94 and 3.89 for *E* isomer and at 3.62 and 3.56 for *Z*-isomer that
384 are perfectly resolved and not overlapping (Figure 5). As indicated in Table 2, upon irradiation
385 at λ_{max} , the *E/Z* ratio change from 100/0 to 47/53 in DMSO and from 92/8 to 25/75 in ethanol.
386 Interestingly, upon irradiation at 300 nm, the reverse, switch back process was not complete
387 and yield *E/Z* ratio of 64/36 in both DMSO and ethanol. Moreover, the photoisomerization was
388 perfectly reversible for at least 5 cycles under consecutive irradiation at 375 or 300 nm,
389 respectively (Figure 6, left) and occurred within several minutes despite the moderate power of
390 the LEDs used as illumination source (see Experimental section: kinetics and Figure 6 right,
391 and SI3 and SI4).



392

393 **Figure 6.** Absorption changes at λ_{\max} during the successive irradiation at two different
 394 wavelengths, 375 and 300 nm (left) and during the $E \rightarrow Z$ photoisomerization process at 375 nm
 395 as a function of time (right).

396

397 Figure 4 shows a typical evolution of the absorption band of 2,6- γ -pyrone upon irradiation at
 398 375 nm in EtOH and DMSO. Additional UV-Vis spectra of the direct and reverse switch in
 399 chloroform and acetonitrile are given in SI. From the kinetic profiles of the direct and reverse
 400 switch (Figure 6 right), one can determine the kinetic parameters such as isomerization half-
 401 life times and rate constants (Table 2). It was observed that the rate constant of the direct $E \rightarrow Z$
 402 switch decreases with increasing the polarity of the solvent, from $30 \cdot 10^{-3} \text{ s}^{-1}$ in chloroform to
 403 $16 \cdot 10^{-3} \text{ s}^{-1}$ in ethanol, except for DMSO, more viscous, for which $k_{E \rightarrow Z}^{375} = 12 \cdot 10^{-3} \text{ s}^{-1}$. On the
 404 contrary, the highest rate constant of the reverse reaction, under irradiation at 300 nm, was
 405 obtained in DMSO, $k_{Z \rightarrow E}^{300} = 182 \cdot 10^{-3} \text{ s}^{-1}$. On the other side, the thermal back-switch was
 406 extremely slow $k_{Z \rightarrow E}^{nr} < 1 \cdot 10^{-6} \text{ s}^{-1}$ at 25°C and only slightly increases to $k_{Z \rightarrow E}^{nr} = 14,7 \cdot 10^{-6} \text{ s}^{-1}$ at
 407 40°C. This negligible thermal switch is of paramount importance for a high temporal control of
 408 the switch, only triggered by irradiation.

409

410 Conclusion

411 In summary, we designed and synthesized a 2,6- γ -pyrone analogue of cyclocurcumin, a
 412 natural photoswitch in the UV-Vis region, in order to improve its photophysical properties and
 413 more particularly to increase the cross-section value of two-photon absorption. Indeed, this

414 feature is compulsory for further *in vivo* applications for which irradiation in the NIR region is
415 needed. To do so, three retrosynthetic pathways were explored. While the passage through an
416 isoxazole intermediate could have been more straightforward and could provide the target final
417 molecule in only 5 steps instead of 10, the corresponding yields were too low (<30 %).
418 Therefore, the pathway involving the cyclization of a diynone was preferred. In this case, we
419 showed that the choice of the starting substrate, guaiacol *vs* propargyl alcohol, is of paramount
420 importance as is conditioning the formation of highly reactive and volatile intermediates such
421 as 2-butynyl aldehyde, if propargyl alcohol is used. Thus, the diynone was build step-by-step,
422 through a bottom-up approach from guaiacol, followed by its cyclization and by the formation
423 of the carbon-carbon double bond *via* an aldolization/crotonization reaction on the residual
424 methylene of the pre-formed pyrone ring. Finally, it was shown that the isomerization of the
425 resulted analogue is a reversible process in which (i) the direct isomerization consists in the
426 transformation of *E*-pyrone into *Z*-pyrone upon irradiation at 375 nm and (ii) the back-switch
427 is the reverse reaction that takes place either by irradiation at 300 nm or thermally, in the dark.
428 The 2,6- γ -pyrone analogue of cyclocurcumin showed excellent photoswitching properties, a
429 low fatigue over at least 5 cycles and a better stability compared to cyclocurcumin. Due to the
430 planar pyrone moiety of the quadrupolar D- π -A- π -D system, the value of two-photon cross-
431 section (159 GM) was higher than the one of cyclocurcumin (14GM), as estimated from DFT
432 calculations. Moreover, we have shown that, differently from CC, photoswitching happens with
433 significant yields rather independently from the solvent polarity. Hence, we believe that our
434 molecular design has tuned the competition between the different relaxation pathways favoring
435 isomerization over fluorescence. All together our results indicate that our designed compound
436 is of interest for further applications as a molecular photoswitch activable via TPA excitation,
437 and hence could be potentially used in biomedical field.

438

439 **Experimental Section**

440 **General**

441 All reactions were carried out under argon atmosphere. Toluene and THF were dried using a
442 MBRAUN MB-SPS-800 solvent purification system. Other solvents and liquid reagents were
443 purified and dried according to recommended procedures. Chemical reagents were purchased
444 from Merck, Fisher Scientific or Sigma-Aldrich and were used as received. Analytical thin-

445 layer chromatography (TLC) analyses were performed using standard procedures on silica gel
446 60 F254 plates (Merck). Compounds were visualized with UV light (254 nm) and alternatively,
447 a potassium permanganate aqueous solution was used. Silica gel column chromatography was
448 performed on a glass column filled with silica gel (63-200 μm) (Merck). Melting points (M.p.)
449 were determined with a Tottoli apparatus and are uncorrected. Spectroscopic analyses and
450 kinetic measurements were carried out on the PhotoNS Platform of the L2CM Laboratory,
451 University of Lorraine. FTIR spectra were recorded on a Shimadzu IRAffinity-1 apparatus
452 equipped with an ATR PIKE Technologies model GladiATR (cm^{-1}). NMR spectra were
453 recorded at 300 K, unless stated otherwise, using a Bruker DRX400 spectrometer (400 MHz
454 for ^1H and 100.6 MHz for ^{13}C). Chemical shifts are reported in ppm (δ) relative to deuterated
455 solvent residual peaks. For complete assignment of ^1H and ^{13}C signals, two-dimensional ^1H , ^1H
456 COSY and ^1H , ^{13}C correlation spectra were recorded. The following abbreviations are used to
457 explain the observed multiplicities: s, singlet; d, doublet; dd, doublet of doublets; ddd, doublet
458 of doublets of doublets; t, triplet; td, triplet of doublets; m, multiplet; bs, broad singlet. High
459 resolutions mass spectra (HRMS) were recorded on a microTOFQ (Bruker) ESI/QqTOF
460 spectrometer.

461

462 **Synthesis**

463 **4-((tert-butyldimethylsilyloxy)-3-methoxybenzaldehyde, 3b:** Vanillin (5.00 g, 32.89 mmol)
464 and 4-dimethylaminopyridine (DMAP) (0.13 g, 1.07 mmol, 3.3 mol%) were combined and
465 dissolved in 100 mL of distilled dichloromethane (DCM) in a clean, dry 250 mL round bottom
466 flask (r.b.f). With continuous flow of dry N_2 gas flushing into the r.b.f., triethylamine (NEt_3)
467 (7.0 mL, 50.50 mmol, 1.54 eq.) were added to the solution and the mixture was cooled to 0°C
468 using an ice/water bath. The *tert*-butyldimethylsilyl chloride (7.42 g, 49.22 mmol, 1.50 eq.) was
469 weighed and added to the reaction mixture portion-wise. Once the addition was completed, the
470 flask was sealed, cooling bath removed and the mixture allowed to stir overnight at room
471 temperature (CCM, SiO_2 , Cyclohexane/EtOAc 95:5). The reaction mixture was quenched by
472 50 mL of cold brine and the organic phase was separated. The aqueous phase was further
473 extracted with DCM (3x50 mL). The combined organic phase was washed with water (3x50
474 mL) and brine (3x50 mL) then dried over Na_2SO_4 , filtered, and evaporated under reduced

475 pressure. Chromatography on silica gel with EtOAc (5%) in cyclohexane afforded the title
476 compound **3b** as a yellowish oil (8.58 g, 98%). ¹H NMR (400 MHz, CDCl₃): δ=9.83 (s, 1H;
477 CHO), 7.39 (d, *J*_{H,H}=1.8 Hz, 1H; Ar-*H*), 7.35 (dd, *J*_{H,H}=8.0, 1.9 Hz, 1H; Ar-*H*), 6.95 (d, *J*_{H,H}=8.0
478 Hz, 1H; Ar-*H*), 3.85 (s, 3H, OCH₃), 0.99 (s, 9H; C(CH₃)₃), 0.18 ppm (s, 6H; Si(CH₃)₂). The
479 NMR data are in agreement with the literature.⁴¹

480 **3-methoxy-4-(methoxymethoxy)benzaldehyde, 3c**: To a stirred solution of vanillin (4.58 g,
481 30.15 mmol) in DCM (120 mL) at 0°C were added DIPEA (10.5 mL, 60.31 mmol, 2.0 eq.) and
482 MOM chloride (3.0 mL, 39.52 mmol, 1.3 eq.). Once the addition was completed, the flask was
483 sealed, cooling bath removed and the mixture allowed to stir one hour at room temperature
484 (CCM, SiO₂, Cyclohexane/EtOAc 7:3). The reaction mixture was quenched with saturated
485 aqueous NH₄Cl (50 mL) and the organic phase was separated. The aqueous phase was further
486 extracted with DCM (3x50 mL). The combined organic phase was washed with water (3x50
487 mL) and brine (3x50 mL) then dried over Na₂SO₄, filtered, and evaporated under reduced
488 pressure. Chromatography on silica gel with EtOAc (20 to 50%) in cyclohexane afforded the
489 title compound **3c** as a yellowish solid (5.83 g, 99%). ¹H NMR (400 MHz, CDCl₃): δ=9.89 (s,
490 1H; CHO), 7.44 (m, 2H; Ar-*H*), 7.30 (d, *J*_{H,H}=8.7 Hz, 1H; Ar-*H*), 5.35 (s, 2H; OCH₂O), 3.97
491 (s, 3H; OCH₃), 3.55 (s, 3H; OCH₃). The NMR data are in agreement with the literature.⁴²

492 **4-(2,2-dibromovinyl)-2-methoxyphenol, 10a**: To a stirred solution of vanillin **3a** (2.05 g,
493 13.44 mmol) and CBr₄ (8.95 g, 26.98 mmol, 2.0 eq.) in dry DCM (40 mL) at 0°C was added
494 fractionally PPh₃ (14.21 g, 54.19 mmol, 4.0 eq.). The mixture was further stirred for 3h at 0°C
495 (CCM, SiO₂, Cyclohexane/EtOAc, 85:15). The reaction mixture was quenched with water (30
496 mL) and the organic phase was separated. The aqueous phase was further extracted with DCM
497 (3x30 mL). The combined organic phases were washed with water (3x30 mL) and brine (3x30
498 mL), then dried over Na₂SO₄, filtered and evaporated under reduced pressure. Purification by
499 chromatography (SiO₂, Cyclohexane/EtOAc, 85:15) afforded compound **10a** as a yellow oil
500 (4.12 g, 99%). *R*_f: 0.38 (Cyclohexane/EtOAc, 85:15); ¹H NMR (400 MHz, CDCl₃): δ=7.39 (s,
501 1H; Ar-*CH*), 7.19 (d, *J*_{H,H}=1.8 Hz, 1H; Ar-*H*), 7.04 (dd, *J*_{H,H}=8.3, 1.9 Hz; Ar-*H*), 6.91 (d,
502 *J*_{H,H}=8.2 Hz, 1H; Ar-*H*), 5.85 (s, 1H; OH), 3.89 (s, 3H; OCH₃); ¹³C{¹H} NMR (100 MHz,
503 CDCl₃): δ=146.3, 146.2, 136.6, 127.5, 122.8, 114.4, 110.6, 87.2, 56.1. ESI-MS (HR) *m/z*:
504 [M+Na]⁺ calcd for C₉H₈Br₂NaO₂: 328,8783, found: 328.8784.

505 **Tert-butyl(4-(2,2-dibromovinyl)-2-methoxyphenoxy)dimethylsilane, 10b**: To a stirred
506 solution of 4-((tert-butyldimethylsilyl)oxy)-3-methoxybenzaldehyde **3b** (2.02 g, 7.57 mmol)
507 and CBr₄ (5.12 g, 15.44 mmol, 2.0 eq.) in dry DCM (40 mL) at 0°C was added PPh₃ (8.36 g,

508 31.89 mmol, 4.2 eq.) fractionally and the mixture was stirred 3h at 0°C (CCM, SiO₂,
509 Cyclohexane/EtOAc 98:2). The reaction mixture was quenched with water (30 mL) and the
510 organic phase was separated. The aqueous phase was further extracted with DCM (3x30 mL).
511 The combined organic phase was washed with water (3x30 mL) and brine (3x30 mL) then dried
512 over Na₂SO₄, filtered and evaporated under reduced pressure. Chromatography on silica gel
513 with EtOAc (2%) in cyclohexane afforded the title compound **10b** as a yellow oil (2.68 g, 84%).
514 *R_f*: 0.39 (Cyclohexane/EtOAc 98:2). ¹H NMR (400 MHz, CDCl₃): δ=7.40 (s, 1H; CH), 7.17
515 (d, *J*_{H,H}=1.8 Hz, 1H; Ar-*H*), 7.01 (dd, *J*_{H,H}=8.3, 1.9 Hz, 1H; Ar-*H*), 6.82 (d, *J*_{H,H}=8.2 Hz, 1H;
516 Ar-*H*), 3.81 (s, 3H; OCH₃), 1.00 (s, 9H; C(CH₃)₃), 0.17 (s, 6H; Si(CH₃)₂). The NMR data are
517 in agreement with the literature.¹⁹

518 **4-(2,2-dibromovinyl)-2-methoxy-1-(methoxymethoxy)benzene, 10c**: To a stirred solution of
519 3-methoxy-4-(methoxymethoxy)benzaldehyde **3c** (503 mg, 2.56 mmol) and CBr₄ (1.72 g, 5.19
520 mmol, 2.0 eq.) in dry DCM (50 mL) at 0°C was added PPh₃ (2.71 g, 10.33 mmol, 4.0 eq.)
521 fractionally and the mixture was stirred 3h at 0°C (CCM, SiO₂, Cyclohexane/EtOAc 95:5). The
522 reaction mixture was quenched with water (30 mL) and the organic phase was separated. The
523 aqueous phase was further extracted with DCM (3x30 mL). The combined organic phase was
524 washed with water (3x30 mL) and brine (3x30 mL) then dried over Na₂SO₄, filtered and
525 evaporated under reduced pressure. Chromatography on silica gel with EtOAc (2%) in
526 cyclohexane afforded the title compound **10c** as a yellow oil (675 mg, 75%). *R_f*: 0.29
527 (Cyclohexane/EtOAc 95:5). ¹H NMR (400 MHz, CDCl₃): δ=7.41 (s, 1H; Ar-CH), 7.19 (d,
528 *J*_{H,H}=1.3 Hz, 1H; Ar-*H*), 7.06 (d, *J*_{H,H}=8.4 Hz, 1H; Ar-*H*), 7.04 (dd, *J*_{H,H}=8.4, 1.3 Hz, 1H; Ar-
529 *H*), 5.24 (s, 2H; OCH₂O), 3.88 (s, 3H; OCH₃), 3.51 (s, 3H; OCH₃). ¹³C{¹H} NMR (100 MHz,
530 CDCl₃): δ=149.4, 146.9, 136.5, 129.6, 122.0, 115.9, 111.8, 95.4, 88.1, 56.4, 56.1. **ESI-MS** (HR)
531 *m/z*: [M+H]⁺ calcd for C₁₁H₁₃Br₂O₃: 350.9226, found: 350.9236; *m/z*: [M+Na]⁺ calcd for
532 C₁₁H₁₂Br₂NaO₃: 372.9045, found: 372.9053.

533 **4-ethynyl-2-methoxyphenol, 5a**: To a stirred solution of 4-(2,2-dibromovinyl)-2-
534 methoxyphenol **10a** (3.00 g, 9.73 mmol) in dry THF (100 mL) at -78°C was added *n*-BuLi (1.4
535 M in THF, 28 mL, 39.20 mmol, 4.0 eq.) dropwise and the mixture was stirred 3h at -78°C
536 (CCM, SiO₂, Cyclohexane/EtOAc 85:15). The reaction mixture was quenched with NH₄Cl (70
537 mL) and the organic phase was separated. The aqueous phase was further extracted with DCM
538 (3x50 mL). The combined organic phase was washed with water (3x50 mL) and brine (3x50
539 mL) then dried over Na₂SO₄, filtered, and evaporated under reduced pressure. Chromatography
540 on silica gel with EtOAc (15%) in cyclohexane afforded the title compound **5a** as a brown oil

541 (1.27 g, 88%). ¹H NMR (400 MHz, CDCl₃): δ=7.06 (dd, *J*_{H,H}=8.2, 1.7 Hz, 1H; Ar-*H*), 6.98 (d,
542 *J*_{H,H}=1.6 Hz, 1H; Ar-*H*), 6.86 (d, *J*_{H,H}=8.2 Hz, 1H; Ar-*H*), 5.83 (s, 1H; OH), 3.87 (s, 3H; OCH₃),
543 2.99 (s, 1H; CH). The NMR data are in agreement with the literature.⁴³

544 **Tert-butyl(4-ethynyl-2-methoxyphenoxy)dimethylsilane, 5b**: To a stirred solution of tert-
545 butyl(4-(2,2-dibromovinyl)-2-methoxyphenoxy)dimethylsilane **10b** (2.35 g, 5.57 mmol) in dry
546 THF (50 mL) at -78°C was added *n*-BuLi (1.4 M in THF, 11 mL, 15.40 mmol, 2.8 eq.) dropwise
547 and the mixture was stirred 3h at -78°C (CCM, SiO₂, Cyclohexane/EtOAc 95:5). The reaction
548 mixture was quenched with NH₄Cl (30 mL) and the organic phase was separated. The aqueous
549 phase was further extracted with DCM (3x30 mL). The combined organic phase was washed
550 with water (3x30 mL) and brine (3x30 mL) then dried over Na₂SO₄, filtered, and evaporated
551 under reduced pressure. Chromatography on silica gel with EtOAc (3%) in cyclohexane
552 afforded the title compound **5b** as an orange oil (1.30 g, 89%). ¹H NMR (400 MHz, CDCl₃):
553 δ=7.00 (dd, *J*_{H,H}=8.1, 1.8 Hz, 1H; Ar-*H*), 6.98 (d, *J*_{H,H}=1.7 Hz, 1H; Ar-*H*), 6.78 (d, *J*_{H,H}=8.0 Hz,
554 1H; Ar-*H*), 3.80 (s, 3H; OCH₃), 2.99 (s, 1H; CH), 0.99 (s, 9H; C(CH₃)₃), 0.16 (s, 6H; Si(CH₃)₂).
555 The NMR data are in agreement with the literature.¹⁸

556 **4-ethynyl-2-methoxy-1-(methoxymethoxy)benzene, 5c**: To a stirred solution of 4-(2,2-
557 dibromovinyl)-2-methoxy-1-(methoxymethoxy)benzene **10c** (150 mg, 0.43 mmol) in dry THF
558 (30 mL) at -78°C was added *n*-BuLi (1.4 M in THF, 0.8 mL, 1.12 mmol, 2.6 eq.) dropwise and
559 the mixture was stirred 3h at -78°C (CCM, SiO₂, Cyclohexane/EtOAc 9:1). The reaction
560 mixture was quenched with NH₄Cl (20 mL) and the organic phase was separated. The aqueous
561 phase was further extracted with DCM (3x20 mL). The combined organic phase was washed
562 with water (3x20 mL) and brine (3x20 mL) then dried over Na₂SO₄, filtered, and evaporated
563 under reduced pressure. Chromatography on silica gel with EtOAc (10%) in cyclohexane
564 afforded the title compound **5c** as a yellow oil (79 mg, 95%). *R*_f: 0.32 (Cyclohexane/EtOAc
565 9:1). ¹H NMR (400 MHz, CDCl₃): δ=7.09-7.05 (m, 2H; Ar-*H*), 7.01 (m, 1H; Ar-*H*), 5.23 (s,
566 2H; OCH₂O), 3.87 (s, 3H; OCH₃), 3.50 (s, 3H; OCH₃), 3.01 (s, 1H; CH). ¹³C{¹H} NMR (100
567 MHz, CDCl₃): δ=149.5, 147.5, 125.6, 116.1, 116.0, 115.5, 95.5, 83.8, 76.1, 56.4, 56.1. **ESI-**
568 **MS** (HR) *m/z*: [M+H]⁺ calcd for C₁₁H₁₃O₃: 193.0859, found: 193.0837; *m/z*: [M+Na]⁺ calcd for
569 C₁₁H₁₂NaO₃: 215.0679, found: 215.0687.

570 **2-methyl-2-(2-nitroethyl)-1,3-dioxolane, 4**: Compound **4** was prepared as previously
571 described in two steps. First, 4-nitrobutan-2-one was prepared by adding dropwise AcOH (6
572 mL, 104.9 mmol, 2.2 eq.) to a mixture of but-3-en-2-one (4 mL, 47.99 mmol) and NaNO₂ (6.86
573 g, 99.46 mmol, 2.1 eq.) in dry THF (50 mL). The mixture was kept under stirring at room

574 temperature overnight and the reaction advancement was followed by CCM (SiO₂,
575 Cyclohexane/EtOAc 1:1). At the end of the reaction, the mixture was diluted with water (50
576 mL) and the organic phase was separated. The aqueous phase was further extracted with EtOAc
577 (3x30 mL). The combined organic phases were washed with water (3x30 mL) and brine (3x30
578 mL) then dried over Na₂SO₄, filtered, and evaporated under reduced pressure. Column
579 chromatography (SiO₂, Cyclohexane/EtOAc, 9:1 to 1:1) afforded the 4-nitrobutan-2-one as a
580 yellow oil (1.93 g, 34%). ¹H NMR (400 MHz, CDCl₃): δ=4.59 (t, *J*_{H,H}=5.9 Hz, 2H; CH₂), 3.07
581 (t, *J*_{H,H}=5.9 Hz, 2H; CH₂-NO₂), 2.23 (s, 3H; CH₃). The NMR data are in agreement with the
582 literature.²¹

583 Then, ethylene glycol (1.2 mL, 21.27 mmol, 12.5 eq.) was added dropwise at room temperature
584 to a stirred solution of 4-nitrobutan-2-one (0.20 g, 1.71 mmol) and pTSA.H₂O (12 mg, 0.06
585 mmol, 0.037 eq.) in dry toluene (5 mL). The mixture was refluxed overnight with a Dean Stark
586 to remove water. The reaction advancement was followed by CCM (SiO₂, Cyclohexane/EtOAc
587 1:1). The reaction mixture was cooled at room temperature and quenched with Na₂CO₃ (5 mL).
588 The organic phase was separated, and the aqueous phase was further extracted with Et₂O (3x5
589 mL). The combined organic phases were washed with water (3x5 mL) and brine (3x5 mL), then
590 dried over Na₂SO₄ and filtered. The filtrate was then purified by chromatography (SiO₂,
591 Cyclohexane/EtOAc, 8:2 to 1:1) to give **4** as a yellow oil (215 mg, 78%). ¹H NMR (400 MHz,
592 CDCl₃): δ=4.44 (t, *J*_{H,H}=7.0 Hz, 2H; CH₂), 3.99-3.91 (m, 4H; CH₂-CH₂), 2.44 (t, *J*_{H,H}=6.9 Hz,
593 2H; CH₂-NO₂), 1.34 (s, 3H; CH₃). The NMR data are in agreement with the literature.²²

594 **2-(prop-2-yn-1-yloxy)tetrahydro-2H-pyran, 12:** To a stirred solution of pTSA.H₂O (0.20 g,
595 1.05 mmol, 0.007 eq.) and DHP (16 mL, 0.175 mol, 1.1 eq.) in dry DCM (150 mL) at room
596 temperature was added propargyl alcohol (**8**) (9.5 mL, 0.161 mol) dropwise and the mixture
597 was stirred 1h at room temperature (CCM, SiO₂, Cyclohexane/EtOAc 9:1). The reaction
598 mixture was quenched with saturated Na₂CO₃ (70 mL) and the organic phase was separated.
599 The aqueous phase was further extracted with DCM (3x50 mL). The combined organic phase
600 was washed with water (3x50 mL) and brine (3x50 mL) then dried over Na₂SO₄, filtered, and
601 evaporated under reduced pressure. Chromatography on silica gel with EtOAc (10%) in
602 cyclohexane afforded the title compound **12** as a yellowish oil (22.11 g, 98%). ¹H NMR (400
603 MHz, CDCl₃): δ=4.81 (m, 1H; O-CH-O), 4.32-4.19 (m, 2H; C-CH₂-O), 3.87-3.80 (m, 1H; O-
604 CH₂-C), 3.55-3.51 (m, 1H; O-CH₂-C), 2.40 (m, 1H; CH), 1.88-1.71 (m, 2H; CH₂), 1.64-1.53
605 (m, 4H; CH₂). The NMR data are in agreement with the literature.²⁶

606 **2-(but-2-yn-1-yloxy)tetrahydro-2H-pyran, 13:** To a stirred solution of 2-(prop-2-yn-1-
607 yloxy)tetrahydro-2H-pyran **12** (11.22 g, 79.9 mmol) in dry THF (200 mL) at -50°C was added
608 *n*-BuLi (1.6M in THF, 62 mL, 99.2 mmol, 1.2 eq.) dropwise and the mixture was stirred 2h at
609 -50°C. The reaction mixture was warmed to 0°C and MeI (10 mL, 160.6 mmol, 2 eq.) was
610 added. The dark brown solution was allowed to warm to room temperature overnight (CCM,
611 SiO₂, Cyclohexane/EtOAc 9:1). The reaction mixture was quenched with saturated NH₄Cl (80
612 mL) and the organic phase was separated. The aqueous phase was further extracted with DCM
613 (3x50 mL). The combined organic phase was washed with water (3x50 mL) and brine (3x50
614 mL) then dried over Na₂SO₄, filtered, and evaporated under reduced pressure. Chromatography
615 on silica gel with EtOAc (10%) in cyclohexane afforded the title compound **13** as a yellow oil
616 (11.69 g, 95%). ¹H NMR (400 MHz, CDCl₃): δ=4.76 (t, *J*_{H,H}=3.3 Hz, 1H; O-CH-O), 4.26-4.10
617 (m, 2H; C-CH₂-O), 3.83-3.77 (m, 1H; O-CH₂-C), 3.51-3.46 (m, 1H; O-CH₂-C), 1.84-1.46 (m,
618 9H). The NMR data are in agreement with the literature.²⁶

619 **But-2-yn-1-ol, 14:** To a stirred solution of 2-(but-2-yn-1-yloxy)tetrahydro-2H-pyran **13** (6.46
620 g, 41.9 mmol) in dry MeOH (50 mL) at room temperature was added pTSA.H₂O (1.00 g, 5.26
621 mmol, 0.126 eq.) and the mixture was stirred over night at room temperature (CCM, SiO₂,
622 Pentane/Et₂O 6:4). The reaction mixture was quenched with saturated Na₂CO₃ (10 mL) and the
623 organic phase was separated. The aqueous phase was further extracted with DCM (3x20 mL).
624 The combined organic phase was washed with water (3x20 mL) and brine (3x20 mL) then dried
625 over Na₂SO₄, filtered, and evaporated under reduced pressure. Chromatography on silica gel
626 with Et₂O (40%) in pentane afforded the title compound **14** as a yellow oil (2.90 g, 99%). ¹H
627 NMR (400 MHz, CDCl₃): δ=4.20 (s, 2H; CH₂), 2.08-1.99 (m, 1H; OH), 1.83 (t, *J*_{H,H}=2.3 Hz,
628 3H; CH₃). The NMR data are in agreement with the literature.²⁶

629 **But-2-ynal, 6:** To a stirred solution of but-2-yn-1-ol **14** (1.01 g, 14.43 mmol) in dry DCM (50
630 mL) at room temperature was added MnO₂ (3.00 g, 34.51 mmol, 2.4 eq.) and the mixture was
631 stirred over night at room temperature (CCM, SiO₂, Pentane/Et₂O 8:2). The reaction mixture
632 was filtered on a celite pad and evaporated under reduced pressure. Chromatography on silica
633 gel with Et₂O (20 to 30%) in pentane afforded the title compound **6** as a yellow oil (641 mg,
634 65%). ¹H NMR (400 MHz, CDCl₃): δ=9.15 (s, 1H; CHO), 2.07 (s, 3H; CH₃). The NMR data
635 are in agreement with the literature.²⁷

636 **4-bromo-2-methoxyphenol, 7:** To a stirred solution of guaiacol **16** (3.00 g, 24.18 mmol) in
637 dry MeCN (150 mL) was slowly added NBS (4.31 g, 24.21 mmol, 1.00 eq.) at 0°C. After
638 stirring for 1h at the same temperature (CCM, SiO₂, Cyclohexane/EtOAc 9:1), the mixture was

639 quenched with saturated aqueous Na₂SO₃ solution (100 mL) and the organic phase was
640 separated. The aqueous phase was further extracted with EtOAc (3x50 mL). The combined
641 organic phase was washed with water (3x50 mL) and brine (3x50 mL) then dried over Na₂SO₄,
642 filtered, and evaporated under reduced pressure. Chromatography on silica gel with EtOAc
643 (10%) in cyclohexane afforded the title compound **7** as a yellow oil (4.51 g, 92%). ¹H NMR
644 (400 MHz, CDCl₃): δ=6.99 (dd, *J*_{H,H}=8.3, 2.2 Hz, 1H; Ar-*H*), 6.97 (d, *J*_{H,H}=2.1 Hz, 1H; Ar-*H*),
645 6.80 (d, *J*_{H,H}=8.3 Hz, 1H; Ar-*H*), 5.64 (br s, 1H; OH), 3.86 (s, 3H; OCH₃). The NMR data are
646 in agreement with the literature.³³

647 **4-bromo-2-methoxy-1-(methoxymethoxy)benzene, 17**: DIPEA (7.60 mL, 43.43 mmol, 2.21
648 eq.) was first added slowly to a stirred solution of 4-bromo-2-methoxyphenol **7** (4.00 g, 19.74
649 mmol) in DCM (100 mL) at 0°C, followed, after few minutes, by the addition dropwise of
650 MOM chloride (2.25 mL, 29.61 mmol, 1.50 eq.). Then, the flask was sealed, the cooling bath
651 was removed, and the stirring was continued for 3h at room temperature (CCM, SiO₂,
652 Cyclohexane/EtOAc, 95:5). The reaction mixture was quenched with saturated aqueous NH₄Cl
653 (50 mL) and the organic phase was separated. The aqueous phase was further extracted with
654 DCM (3x50 mL) and the combined organic phases were washed with water (3x50 mL) and
655 brine (3x50 mL), then dried over Na₂SO₄, filtered, and evaporated under reduced pressure.
656 Chromatography (SiO₂, Cyclohexane/EtOAc, 95:5 to 9:1) afforded the protected compound **17**
657 as a yellowish oil (4.73 g, 97%). ¹H NMR (400 MHz, CDCl₃): δ=7.01 (m, 3H; Ar-*H*), 5.19 (s,
658 2H; OCH₂O), 3.86 (s, 3H; OCH₃), 3.50 (s, 3H; OCH₃). The NMR data are in agreement with
659 the literature.³²

660 **3-(3-methoxy-4-(methoxymethoxy)phenyl)prop-2-yn-1-ol, 18**: To a stirred solution of 4-
661 bromo-2-methoxy-1-(methoxymethoxy)benzene **17** (3.80 g, 15.39 mmol) in diisopropylamine
662 (*i*Pr₂NH, 80 mL) was added PdCl₂(PPh₃)₂ (0.22g, 0.32 mmol, 0.02 eq.), CuI (0.12 g, 0.62 mmol,
663 0.04 eq.) and PPh₃ (0.16g, 0.62 mmol, 0.04 eq.). The solution was extensively degassed by
664 argon bubbling. Propargyl alcohol (**8**) (1.20 mL, 20.32 mmol, 1.32 eq.) was added and the
665 mixture was stirred overnight at 80°C (CCM, SiO₂, Cyclohexane/EtOAc, 3:1). After cooling
666 and filtration on a short pad of silica gel eluted with EtOAc, the resulting filtrate was washed
667 with water (3x50 mL) and brine (3x50 mL), then dried over Na₂SO₄, filtered, and purified by
668 chromatography (SiO₂, Cyclohexane/EtOAc, 8:2 to 1:1) to afford the compound **18** as a brown
669 oil (3.14 g, 92%). *R*_f: 0.27 (Cyclohexane/EtOAc, 1:1). *IR* (ATR, cm⁻¹): ν: 3385 (OH), 2230. ¹H
670 NMR (400 MHz, CDCl₃): δ=7.08 (d, *J*_{H,H}=8.3 Hz, 1H; Ar-*H*), 7.00 (dd, *J*_{H,H}=8.3, 1.8 Hz, 1H;
671 Ar-*H*), 6.97 (d, *J*_{H,H}=1.8 Hz, 1H; Ar-*H*), 5.23 (s, 2H; OCH₂O), 4.49 (d, *J*_{H,H}=4.8 Hz, 2H; CH₂),

672 3.87 (s, 3H; OCH₃), 3.51 (s, 3H; OCH₃), 2.27 (br s, 1H; OH). ¹³C{¹H} NMR (100 MHz,
673 CDCl₃): δ=149.4, 147.1, 125.0, 116.5, 116.0, 115.0, 95.4, 86.3, 85.5, 56.4, 56.0, 51.6. ESI-MS
674 (HR) *m/z*: [M+H]⁺ calcd for C₁₂H₁₅O₄: 223.0965, found: 223.0917; *m/z*: [M+Na]⁺ calcd for
675 C₁₂H₁₄NaO₄: 245.0784, found: 245.0730.

676 **3-(3-methoxy-4-(methoxymethoxy)phenyl)propionaldehyde, 19**: A suspension of MnO₂
677 (11.80 g, 0.136 mol, 10 eq.) in dry DCM (120 mL) was added to 3-(3-methoxy-4-
678 (methoxymethoxy)phenyl)prop-2-yn-1-ol **18** (3.02 g, 13.61 mmol) and stirred overnight at
679 room temperature (CCM, SiO₂, Cyclohexane/EtOAc, 3:1). Filtration on a short pad of silica gel
680 eluted with DCM gave a filtrate which was concentrated and chromatographed (SiO₂,
681 Cyclohexane/EtOAc, 75:25) to afford compound **19** as a brown oil (2.79 g, 93%). *R_f*: 0.37
682 (Cyclohexane/EtOAc, 3:1). IR (ATR, cm⁻¹): 2176, 1647 (CH=O). ¹H NMR (400 MHz,
683 CDCl₃): δ=9.39 (s, 1H; CHO), 7.22 (dd, *J*_{H,H}=8.4, 1.9 Hz, 1H; Ar-*H*), 7.15 (d, *J*_{H,H}=8.4 Hz, 1H;
684 Ar-*H*), 7.11 (d, *J*_{H,H}=1.8 Hz, 1H; Ar-*H*), 5.28 (s, 2H; OCH₂O), 3.89 (s, 3H; OCH₃), 3.51 (s, 3H;
685 OCH₃). ¹³C{¹H} NMR (100 MHz, CDCl₃): δ=176.8, 149.8, 149.6, 127.7, 116.2, 115.8, 112.8,
686 96.3, 95.3, 88.5, 56.6, 56.2. ESI-MS (HR) *m/z*: [M+H]⁺ calcd for C₁₂H₁₃O₄: 221.0808, found:
687 221.0738; *m/z*: [M+Na]⁺ calcd for C₁₂H₁₂NaO₄: 243.0628, found: 243.0563.

688 **1-(3-methoxy-4-(methoxymethoxy)phenyl)hexa-1,4-diyne-3-ol, 15**: To a solution of 3-(3-
689 methoxy-4-(methoxymethoxy)phenyl)propionaldehyde **19** (0.33 g, 1.50 mmol) in anhydrous
690 THF (5 mL) was added 1-propynylmagnesium bromide (**9**) (0.50M solution in THF, 4.50 mL,
691 2.25 mmol, 1.50 eq.) at -20°C and stirred for 0.5h. Stirring was maintained for another 1h at
692 room temperature (CCM, SiO₂, Cyclohexane/EtOAc, 4:1). The reaction mixture was then
693 quenched with saturated aqueous NH₄Cl (3 mL) and the organic phase was separated. The
694 aqueous phase was further extracted with DCM (3x5 mL) and the combined organic phases
695 were washed with water (3x5 mL) and brine (3x5 mL), then dried over Na₂SO₄ and filtered.
696 The concentrated filtrate was purified by chromatography (SiO₂, Cyclohexane/EtOAc, 8:2 to
697 1:1) to afford the diyne **15** as a yellow oil (0.347 g, 89%). *R_f*: 0.22 (Cyclohexane/EtOAc, 4:1).
698 IR (ATR, cm⁻¹): 3354 (OH), 2181. ¹H NMR (400 MHz, CDCl₃): δ=7.06 (d, *J*_{H,H}=8.3 Hz, 1H;
699 Ar-*H*), 7.01 (dd, *J*_{H,H}=8.3, 1.8 Hz, 1H; Ar-*H*), 6.98 (d, *J*_{H,H}=1.7 Hz, 1H; Ar-*H*), 5.30 (br s, 1H;
700 OH), 5.22 (s, 2H; OCH₂O), 3.85 (s, 3H; OCH₃), 3.49 (s, 3H; OCH₃), 2.52 (d, *J*_{H,H}=5.0 Hz, 1H;
701 CH), 1.88 (d, *J*_{H,H}=2.2 Hz, 3H; CH₃). ¹³C{¹H} NMR (100 MHz, CDCl₃): δ=149.4, 147.5, 125.3,
702 116.0, 115.9, 115.2, 95.5, 85.5, 84.1, 83.3, 81.6, 56.5, 56.1, 53.0, 3.9. ESI-MS (HR) *m/z*:
703 [M+H]⁺ calcd for C₁₅H₁₇O₄: 261.1121, found: 261.1136; *m/z*: [M+Na]⁺ calcd for C₁₅H₁₆NaO₄:
704 283.0941, found: 283.1018.

705 **1-(3-methoxy-4-(methoxymethoxy)phenyl)hexa-1,4-diyne-3-one, 20:** MnO₂ (9.49 g, 0.109
706 mol, 20 eq.) was added into a solution of 1-(3-methoxy-4-(methoxymethoxy)-phenyl)-
707 propionaldehyde **15** (1.41 g, 5.43 mmol) in dry DCM (50 mL). The mixture was stirred
708 overnight at room temperature (CCM, SiO₂, Cyclohexane/EtOAc, 4:1). The reaction mixture
709 was then filtered on a short pad of silica gel eluted with DCM, the resulting filtrate was
710 concentrated and purified by chromatography (SiO₂, Cyclohexane/EtOAc, 85:25) to give the
711 diyne **20** as a brown oil (1.36 g, 97%). *R_f*: 0.31 (Cyclohexane/EtOAc, 4:1). **IR** (KBr): 2181,
712 1616 (C=O). **¹H NMR** (400 MHz, CDCl₃): δ=7.23 (dd, *J*_{H,H}=8.4, 1.9 Hz, 1H; Ar-*H*), 7.14 (d,
713 *J*_{H,H}=8.4 Hz, 1H; Ar-*H*), 7.12 (d, *J*_{H,H}=1.8 Hz, 1H; Ar-*H*), 5.28 (s, 2H; OCH₂O), 3.89 (s, 3H;
714 OCH₃), 3.51 (s, 3H; OCH₃), 2.10 (s, 3H; CH₃). **¹³C{¹H} NMR** (100 MHz, CDCl₃): δ=161.0,
715 149.7, 149.5, 127.8, 116.0, 115.7, 112.8, 95.3, 91.6, 91.4, 89.3, 81.6, 56.6, 56.2, 4.5. **ESI-MS**
716 (HR) *m/z*: [M+H]⁺ calcd for C₁₅H₁₅O₄: 259.0965, found: 259.0979; *m/z*: [M+Na]⁺ calcd for
717 C₁₅H₁₄NaO₄: 281.0784, found: 281.0807.

718 **2-(4-hydroxy-3-methoxyphenyl)-6-methyl-4H-pyran-4-one, 2:** TfOH (2.4 μL, 27.12 mmol,
719 1.0 eq.) was added dropwise to a solution of 1-(3-methoxy-4-(methoxymethoxy)phenyl)hexa-
720 1,4-diyne-3-one **20** in deionized water (77 mL) and the mixture was stirred 4h at 100°C (CCM,
721 SiO₂, EtOAc/MeOH, 9:1). After cooling to room temperature, the reaction mixture was diluted
722 with water (20 mL) and EtOAc (20 mL). The organic phase was separated, and the aqueous
723 phase was further extracted with EtOAc (3x20 mL). The combined organic phases were washed
724 with water (3x20 mL) and brine (3x20 mL), then dried over Na₂SO₄ and filtered. The filtrate
725 was chromatographed (SiO₂, EtOAc/MeOH, 9:1) and afforded compound **2** as a white solid
726 (4.95 g, 79%). *R_f*: 0.34 (EtOAc/MeOH, 9:1). **M.p.**: 112°C. **IR** (ATR, cm⁻¹): 3410, 1651, 1645,
727 1520, 856. **UV-Vis** (DMSO): 316 nm. **¹H NMR** (400 MHz, CDCl₃): δ=7.33 (dd, *J*_{H,H}=8.4, 2.1
728 Hz, 1H; Ar-*H*), 7.19 (d, *J*_{H,H}=2.1 Hz, 1H; Ar-*H*), 7.00 (d, *J*_{H,H}=8.4 Hz, 1H; Ar-*H*), 6.62 (d,
729 *J*_{H,H}=2.2 Hz, 1H; *H*_{pyrone}), 6.17 (dd, *J*_{H,H}=2.0, 0.6 Hz, 1H; *H*_{pyrone}), 3.95 (s, 3H; OCH₃), 2.37 (d,
730 *J*_{H,H}=0.5 Hz, 3H; CH₃). **¹³C{¹H} NMR** (100 MHz, CDCl₃): δ=180.6, 165.4, 164.0, 149.1, 147.2,
731 123.4, 120.2, 115.2, 114.2, 109.5, 108.2, 56.2, 20.0. **ESI-MS** (HR) *m/z*: [M+H]⁺ calcd for
732 C₁₃H₁₃O₄: 233.0808, found: 233.0902; *m/z*: [M+Na]⁺ calcd for C₁₃H₁₂NaO₄: 255.0628, found:
733 255.0611.

734 **2-(3-methoxy-4-(methoxymethoxy)phenyl)-6-methyl-4H-pyran-4-one, 21:** To a solution of
735 2-(4-hydroxy-3-methoxyphenyl)-6-methyl-4H-pyran-4-one **2** (40 mg, 0.17 mmol) in DCM (5
736 mL) were added DIPEA (67 μL, 0.26 mmol, 1.50 eq.) and MOM chloride (20 μL, 0.38 mmol,
737 2.21 eq.) under stirring at 0°C. After addition, the flask was sealed and the mixture was stirred

738 for 3h at room temperature (CCM, SiO₂, EtOAc). The reaction mixture was quenched with
739 saturated aqueous NH₄Cl (3 mL) and the organic phase was separated. The aqueous phase was
740 further extracted with DCM (3x5 mL). The combined organic phases were washed with water
741 (3x5 mL) and brine (3x5 mL), then dried over Na₂SO₄, filtered, concentrated, and purified by
742 chromatography (SiO₂, EtOAc) to afford the protected derivative **21** as a white solid (47 mg,
743 98%). *R_f*: 0.30 (EtOAc). *M.p.*: 158°C. **IR** (ATR, cm⁻¹): 1655, 1612, 1512, 858. **UV-Vis**
744 (DMSO): 310 nm. **¹H NMR** (400 MHz, CDCl₃): δ=7.29 (dd, *J*_{H,H}=8.5, 2.2 Hz, 1H; Ar-*H*), 7.19
745 (d, *J*_{H,H}=2.1 Hz, 1H; Ar-*H*), 7.17 (d, *J*_{H,H}=8.5 Hz, 1H; Ar-*H*), 6.57 (d, *J*_{H,H}=2.2 Hz, 1H; *H*_{pyrone}),
746 6.10 (dd, *J*_{H,H}=2.1, 0.7 Hz, 1H; *H*_{pyrone}), 5.23 (s, 2H; OCH₂O), 3.89 (s, 3H; OCH₃), 3.47 (s, 3H;
747 OCH₃), 2.32 (d, *J*_{H,H}=0.6 Hz, 3H; CH₃). **¹³C{¹H} NMR** (100 MHz, CDCl₃): δ=180.2, 165.2,
748 163.4, 149.9, 149.2, 125.3, 119.2, 115.9, 114.2, 109.9, 109.0, 95.2, 56.4, 56.1, 19.9. **ESI-MS**
749 (HR) *m/z*: [M+H]⁺ calcd for C₁₅H₁₇O₅: 277.1071, found: 277.1088; *m/z*: [M+Na]⁺ calcd for
750 C₁₅H₁₆NaO₅: 299.0890, found: 299.0899.

751 **(*E*)-2-(3-methoxy-4-(methoxymethoxy)phenyl)-6-(3-methoxy-4-(methoxymethoxy)styryl)**
752 **-4H-pyran-4-one, 22**: A freshly prepared NaOEt solution (1.478 M in EtOH, 2.2 mL, 3.25
753 mmol, 1.79 eq.) was added dropwise to a mixture of 2-(3-methoxy-4-
754 (methoxymethoxy)phenyl)-6-methyl-4H-pyran-4-one **21** (500 mg, 1.81 mmol) and 3-methoxy-
755 4-(methoxymethoxy) benzaldehyde **3c** (510 mg, 2.59 mmol, 1.43 eq.) in dry EtOH (20 mL) at
756 room temperature. Then the mixture was warmed to 40°C and stirred for 48h (CCM, SiO₂,
757 EtOAc). The reaction was quenched with water (10 mL) and the crude product was extracted
758 with DCM (4x10 mL). The combined organic phases were washed with water (3x10 mL) and
759 brine (3x10 mL), then dried over Na₂SO₄ and filtered. The concentrated filtrate was purified on
760 column chromatography (SiO₂, EtOAc) to give the title compound **22** as a yellow solid (310
761 mg, 38%). *R_f*: 0.28 (EtOAc). *M.p.*: 131°C. **IR** (ATR, cm⁻¹): 3076, 2932, 1645, 1628, 1599,
762 1504. **UV-Vis** (DMSO): 356 nm. **¹H NMR** (400 MHz, CDCl₃): δ=7.46 (dd, *J*_{H,H}=8.5, 2.0 Hz,
763 1H; Ar-*H*), 7.42 (d, *J*_{H,H}=16.0 Hz, 1H; *H*_β), 7.31 (d, *J*_{H,H}=1.6 Hz, 1H; Ar-*H*), 7.30 (d, *J*_{H,H}=8.4
764 Hz, 1H; Ar-*H*), 7.19 (d, *J*_{H,H}=8.1 Hz, 1H; Ar-*H*), 7.09 (m, 2H; Ar-*H*), 6.70 (d, *J*_{H,H}=1.9 Hz, 1H;
765 *H*_{pyrone}), 6.67 (d, *J*_{H,H}=16.0 Hz, 1H; *H*_α), 6.31 (d, *J*_{H,H}=1.8 Hz, 1H; *H*_{pyrone}), 5.32 (s, 2H; OCH₂O),
766 5.28 (s, 2H; OCH₂O), 3.98 (s, 3H; OCH₃), 3.97 (s, 3H; OCH₃), 3.54 (s, 3H; OCH₃), 3.53 (s,
767 3H; OCH₃). **¹³C{¹H} NMR** (100 MHz, CDCl₃): δ=180.3, 162.8, 161.8, 150.1, 150.0, 149.4,
768 148.3, 135.8, 129.4, 125.6, 121.7, 119.5, 118.3, 116.1, 116.0, 113.5, 110.5, 109.9, 109.3, 95.3,
769 95.2, 56.4, 56.1. **ESI-MS** (HR) *m/z*: [M+H]⁺ calcd for C₂₅H₂₇O₈: 455.1700, found: 455.1696;

770 m/z : $[M+Na]^+$ calcd for $C_{25}H_{26}NaO_8$: 477.1520, found: 477.1471; m/z : $[M+K]^+$ calcd for
771 $C_{25}H_{26}KO_8$: 493.1259, found: 493.1220.

772 **(E)-2-(4-hydroxy-3-methoxyphenyl)-6-(4-hydroxy-3-methoxystyryl)-4H-pyran-4-one, 1:**

773 To a stirred solution of (E)-2-(3-methoxy-4-(methoxymethoxy)phenyl)-6-(3-methoxy-4-
774 (methoxymethoxy)styryl)-4H-pyran-4-one **22** (170 mg, 0.37 mmol) in MeOH (10 mL) it was
775 added dropwise, at room temperature, an excess of HCl 1M (3 mL, 3.00 mmol, 8.02 eq.). The
776 mixture was then refluxed for 3h and the reaction advancement was followed by CCM (SiO₂,
777 EtOAc/MeOH, 95:5). At the end, the reaction was quenched with water (10 mL), the
778 precipitated product was filtered, washed with water, and finally dried to afford the 2,6- γ -
779 pyrone **1** as a yellow solid (125 mg, 91%). *R_f*: 0.33 (EtOAc/MeOH, 95:5). *M.p.*: 238 °C. **IR**
780 (ATR, cm⁻¹): 3134 (br), 2932, 1641, 1628, 1595, 1508. **¹H NMR** (400 MHz, DMSO-*d*₆):
781 δ =9.87 (s, 1H; OH), 9.56 (s, 1H; OH), 7.58 (dd, $J_{H,H}$ =8.3, 2.2 Hz, 1H; Ar-*H*), 7.52 (d, $J_{H,H}$ =16.1
782 Hz, 1H; *H_β*), 7.52 (d, $J_{H,H}$ =2.1 Hz, 1H; Ar-*H*), 7.37 (d, $J_{H,H}$ =1.9 Hz, 1H; Ar-*H*), 7.19 (dd,
783 $J_{H,H}$ =8.3, 1.9 Hz, 1H; Ar-*H*), 7.01 (d, $J_{H,H}$ =16.1 Hz, 1H; *H_α*), 6.99 (d, $J_{H,H}$ =8.3 Hz, 1H; Ar-*H*),
784 6.86 (d, $J_{H,H}$ =7.8 Hz, 1H; Ar-*H*), 6.85 (d, $J_{H,H}$ =2.1 Hz, 1H; *H_{pyrone}*), 6.32 (d, $J_{H,H}$ =2.2 Hz, 1H;
785 *H_{pyrone}*), 3.94 (s, 3H; OCH₃), 3.89 (s, 3H; OCH₃). **¹³C{¹H} NMR** (100 MHz, DMSO-*d*₆):
786 δ =180.0, 163.2, 162.6, 151.0, 149.6, 149.0, 148.95, 136.7, 127.7, 123.3, 122.9, 120.7, 117.9,
787 116.8, 116.6, 113.2, 111.8, 110.7, 109.8, 56.8, 56.7. **ESI-MS** (HR) m/z : $[M+H]^+$ calcd for
788 $C_{21}H_{19}O_6$: 367.1176, found: 367.1260; m/z : $[M+Na]^+$ calcd for $C_{21}H_{18}NaO_6$: 389.0996, found:
789 389.0967; m/z : $[M+K]^+$ calcd for $C_{21}H_{18}KO_6$: 405.0735, found: 405.0684.

790 **(Z)-2-(4-hydroxy-3-methoxyphenyl)-6-(4-hydroxy-3-methoxystyryl)-4H-pyran-4-one, 1:**

791 An irradiation at 375 nm of the solution of **1** in DMSO led to **1'** with a ratio: **1/1' 47:53**. **¹H**
792 **NMR** (400 MHz, DMSO-*d*₆): δ =9.58 (s, 1H; OH), 9.36 (s, 1H; OH), 7.00 (d, $J_{H,H}$ =1.5 Hz, 1H;
793 Ar-*H*), 6.97 (d, $J_{H,H}$ =1.9 Hz, 1H; Ar-*H*), 6.94 (d, $J_{H,H}$ =12.0 Hz, 1H; *H_β*), 6.88 (m, 1H; Ar-*H*),
794 6.83 (d, $J_{H,H}$ =2.2 Hz, 1H; *H_{pyrone}*), 6.80 (dd, $J_{H,H}$ =8.4, 2.1 Hz, 1H; Ar-*H*), 6.77 (d, $J_{H,H}$ =8.1 Hz,
795 1H; Ar-*H*), 6.70 (d, $J_{H,H}$ =8.4 Hz, 1H; Ar-*H*), 6.33 (d, $J_{H,H}$ =2.6 Hz, 1H; *H_{pyrone}*), 6.32 (d,
796 $J_{H,H}$ =12.0 Hz, 1H; *H_α*), 3.62 (s, 3H; OCH₃), 3.56 (s, 3H; OCH₃). **¹³C{¹H} NMR** (100 MHz,
797 DMSO-*d*₆): δ =179.7, 163.3, 162.5, 150.8, 148.6, 148.4, 148.2, 138.7, 127.9, 123.5, 122.3,
798 120.5, 119.5, 116.3, 116.2, 115.7, 113.7, 110.1, 109.7, 56.3, 56.2. **ESI-MS** (HR) m/z : $[M+H]^+$
799 calcd for $C_{21}H_{19}O_6$: 367.1176, found: 367.1199; m/z : $[M+Na]^+$ calcd for $C_{21}H_{18}NaO_6$:
800 389.0996, found: 389.0969; m/z : $[M+K]^+$ calcd for $C_{21}H_{18}KO_6$: 405.0735, found: 405.0718.

801

802 **Computational methodology**

803 Ground state minima of both isomers of the prepared 2,6- γ -pyrone analogue of cyclocurcumin
804 **1** was found under the framework of the density functional theory (DFT), applying the B3LYP
805 functional.⁴⁴

806 To compute the absorption spectra of both isomers, the time-dependent DFT (TD-DFT) was
807 used. Different DFT functionals and basis sets were used to characterize the excitation of the
808 molecule using the Gaussian16 software.⁴⁵ As more remarkable, two main behaviors can be
809 shown. The CAM-B3LYP strongly blueshifts the absorption maximum as is common for range-
810 separate functionals.⁴⁶ It can be related to an improved representation of charge-transfer states
811 compared to hybrid functionals that avoids the presence of significant intruder states, whose
812 excitation energy would have been artificially lowered. In contrast, B3LYP better describes the
813 shape of the absorption spectrum but yields in the presence of intruder states due to an
814 overstabilization of the S₃ and an increase of the charge transfer states.⁴⁴

815 To provide UV data more accurate to the one found experimentally, the vibrational and
816 dynamical effects were considered around Franck-Condon region *via* a Wigner distribution,
817 using the NewtonX code to generate 100 structures.⁴⁷ Excited states were computed for each
818 one through single point calculations in vacuum at the CAM-B3LYP/6-31G* level of theory
819 considering 20 roots, and finally convoluting all the Gaussian functions resulting from all
820 transition energies and oscillator strengths.⁴⁸ Furthermore, this was done for the molecule in
821 different solvents, using the optimized structure and the phase space for each solvent, not the
822 vacuum frequencies. The solvent was included using the polarizable continuum model (PCM)⁴⁹
823 as implemented in Gaussian16,⁴⁵ using water, ethanol, dimethyl sulfoxide, and chloroform.

824 Fluorescence spectrum in vacuo was obtained from a Wigner distribution, sampling the
825 vibrational space on the excited state minimum generating 100 structures. To compute the
826 emission spectra, the first root which represents the S₀ to S₁ transition was only considered.

827 Coherently with an established protocol⁵⁰⁻⁵³ TPA cross section have been simulated as
828 vertical transition from the ground-state equilibrium geometry only, *i.e.* the Franck-Condon

829 region, and was obtained at TD-DFT level of theory through a quadratic response approach as
830 implemented in DALTON package.⁵⁴ CAM-B3LYP exchange-correlation functional and the
831 Pople 6-311++G(d,p) basis set were used, while excitation energies and cross-sections have
832 been calculated considering the effect of water solvent modeled at PCM level.

833 **Steady-state measurements**

834 **Absorption and emission spectra.** UV-visible spectra were recorded on a Perkin-
835 Elmer Lambda 1050 UV-vis-NIR spectrophotometer using a 1 cm optical path length cell at
836 25°C, unless otherwise specified. The steady state measurements were recorded on a Jobin
837 Yvon Fluorolog-3 spectrofluorometer from Horiba Scientific and the FluorEssence program.
838 The excitation source was a 450 W xenon lamp, and the detector used was an R-928 operating
839 at a voltage of 950 V. Excitation and emission slits width were 1 nm. The fluorescence quantum
840 yields were determined using quinine sulphate as a standard ($\Phi = 0.53$ in H₂SO₄, 0.05M) using

$$841 \quad \Phi_x = \Phi_s \left(\frac{Grad_x}{Grad_s} \right) \left(\frac{\eta_x^2}{\eta_s^2} \right)$$

842 where Φ , Grad and η represent fluorescence quantum yield, gradient from the plot of integrated
843 fluorescence intensity vs. absorbance, and refractive index of the solvent, respectively. The
844 subscripts S and X denote standard and test, respectively.

845 **Kinetics and fatigue resistance.** The photo-isomerization was carried out on a 1.0 cm-path-
846 length quartz cell places on a 4-sided cuvette holder (Cuvette Holder with Four Light Ports,
847 CVH100 Thorlabs). Unless otherwise specified, the concentration of the samples was of 40
848 μ M. The kinetics of the photoisomerization process were measured by following the absorption
849 spectrum during irradiation by selected light-emitting diodes (LED), placed perpendicular to
850 the absorbance measurement. To reach the photostationary state of the $E \rightarrow Z$ isomerization, the
851 E-stereoisomer was illuminated within the $\pi-\pi^*$ band using a M375L4.1540 mW LED (LED
852 Power Output 1540mW, 2% power used) with a central wavelength of 375 nm and a bandwidth
853 (FWHM) of 9 nm. For the reverse transformation, $Z \rightarrow E$ isomerization, the compound was
854 excited within the $n-\pi^*$ band using a M300L4.32 mW LED (LED Power Output: 47mW, full
855 power used) with a central wavelength of 300 nm with a bandwidth (FWHM) of 20 nm. In this
856 case, the concentrations of the compound **22** were of 28.5 μ M in DMSO, 33 μ M in ethanol,
857 27 μ M in acetonitrile and 24 μ M in chloroform. The thermal return process between Z and E
858 isomers was analyzed by measuring the changes of the maximum absorbance wavelength at 25

859 and 40°C, respectively. Kinetic monitoring of absorbance was performed using an Ocean
860 Optics USB2000 + XR CCD sensor and kinetic constants were determined using “Biokine”
861 software.

862

863 Acknowledgements

864 JP acknowledges the French Ministry of Higher Education, Research and Innovation for his
865 PhD grant. The authors greatly acknowledge the NMR Plateforme of Jean Barriol Institut, and
866 MassLor Spectrometry Plateforme of the University of Lorraine. The authors thank F. Dupire
867 for performing mass spectrometry measurements. The authors gratefully acknowledge
868 University of Lorraine, CNRS and the European Regional Development Funds (Programme
869 opérationnel FEDER-FSE Lorraine et Massif des Vosges 2014-2020/”Fire Light” project:
870 “Photo-bio-active molecules and nanoparticles”) for financial support.

871

872 References

- 873 (1) Gozem, S.; Schapiro, I.; Ferre, N.; Olivucci, M. The Molecular Mechanism of Thermal Noise in
874 Rod Photoreceptors. *Science* **2012**, *337* (6099), 1225–1228.
875 <https://doi.org/10.1126/science.1220461>.
- 876 (2) Marazzi, M.; Gattuso, H.; Giussani, A.; Zhang, H.; Navarrete-Miguel, M.; Chipot, C.; Cai, W.;
877 Roca-Sanjuán, D.; Dehez, F.; Monari, A. Induced Night Vision by Singlet-Oxygen-Mediated
878 Activation of Rhodopsin. *J. Phys. Chem. Lett.* **2019**, *10* (22), 7133–7140.
879 <https://doi.org/10.1021/acs.jpcclett.9b02911>.
- 880 (3) Sampedro, D.; Migani, A.; Pepi, A.; Busi, E.; Basosi, R.; Latterini, L.; Elisei, F.; Fusi, S.; Ponticelli,
881 F.; Zanirato, V.; Olivucci, M. Design and Photochemical Characterization of a Biomimetic Light-
882 Driven Z/E Switcher. *J. Am. Chem. Soc.* **2004**, *126* (30), 9349–9359.
883 <https://doi.org/10.1021/ja038859e>.
- 884 (4) Bresolí-Obach, R.; Massad, W. A.; Abudulimu, A.; Lüer, L.; Flors, C.; Luis, J. G.; Rosquete, L. I.;
885 Grillo, T. A.; Anamimoghadam, O.; Bucher, G.; Nonell, S. 9-Aryl-Phenalenones: Bioinspired
886 Thermally Reversible Photochromic Compounds for Photoswitching Applications in the Pico-to
887 Milliseconds Range. *Dyes and Pigments* **2021**, *186*, 109060.
888 <https://doi.org/10.1016/j.dyepig.2020.109060>.
- 889 (5) Romero, M. A.; Mateus, P.; Matos, B.; Acuña, Á.; García-Río, L.; Arteaga, J. F.; Pischel, U.; Basílio,
890 N. Binding of Flavylum Ions to Sulfonatocalix[4]Arene and Implication in the Photorelease of
891 Biologically Relevant Guests in Water. *J. Org. Chem.* **2019**, *84* (17), 10852–10859.
892 <https://doi.org/10.1021/acs.joc.9b01420>.
- 893 (6) Marazzi, M.; Francés-Monerris, A.; Mourer, M.; Pasc, A.; Monari, A. Trans-to-Cis
894 Photoisomerization of Cyclocurcumin in Different Environments Rationalized by Computational
895 Photochemistry. *Phys. Chem. Chem. Phys.* **2020**, *22* (8), 4749–4757.
896 <https://doi.org/10.1039/C9CP06565B>.

- 897 (7) Adhikary, R.; Barnes, C. A.; Trampel, R. L.; Wallace, S. J.; Kee, T. W.; Petrich, J. W. Photoinduced
898 Trans-to-Cis Isomerization of Cyclocurcumin. *J. Phys. Chem. B* **2011**, *115* (36), 10707–10714.
899 <https://doi.org/10.1021/jp200080s>.
- 900 (8) Albota, M.; Beljonne, D.; Brédas, J. L.; Ehrlich, J. E.; Fu, J. Y.; Heikal, A. A.; Hess, S. E.; Kogej, T.;
901 Levin, M. D.; Marder, S. R.; McCord-Maughon, D.; Perry, J. W.; Röckel, H.; Rumi, M.;
902 Subramaniam, G.; Webb, W. W.; Wu, X. L.; Xu, C. Design of Organic Molecules with Large Two-
903 Photon Absorption Cross Sections. *Science* **1998**, *281* (5383), 1653–1656.
904 <https://doi.org/10.1126/science.281.5383.1653>.
- 905 (9) Light, R. J.; Hauser, C. R. Aroylations of β -Diketones at the Terminal Methyl Group to Form
906 1,3,5-Triketones. Cyclizations to 4-Pyrones and 4-Pyridones. *J. Org. Chem.* **1960**, *25* (4), 538–
907 546. <https://doi.org/10.1021/jo01074a013>.
- 908 (10) Knight, J. D.; Metz, C. R.; Beam, C. F.; Pennington, W. T.; VanDerveer, D. G. New Strong Base
909 Synthesis of Symmetrical 1,5-Diaryl-1,3,5-Pentanetriones from Acetone and Benzoate Esters.
910 *Synthetic Communications* **2008**, *38* (14), 2465–2482.
911 <https://doi.org/10.1080/00397910802138488>.
- 912 (11) Solas, M.; Muñoz, M. A.; Suárez-Pantiga, S.; Sanz, R. Regiodivergent Hydration–Cyclization of
913 Diynones under Gold Catalysis. *Org. Lett.* **2020**, *22* (19), 7681–7687.
914 <https://doi.org/10.1021/acs.orglett.0c02892>.
- 915 (12) Xu, Y.-L.; Teng, Q.-H.; Tong, W.; Wang, H.-S.; Pan, Y.-M.; Ma, X.-L. Atom-Economic Synthesis of
916 4-Pyrones from Diynones and Water. *Molecules* **2017**, *22* (1), 109.
917 <https://doi.org/10.3390/molecules22010109>.
- 918 (13) Habert, L.; Cariou, K. Photoinduced Aerobic Iodoarene-Catalyzed Spirocyclization of *N*-Oxy-
919 amides to *N*-Fused Spirolactams**. *Angew. Chem.* **2021**, *133* (1), 173–177.
920 <https://doi.org/10.1002/ange.202009175>.
- 921 (14) Li, C.-S.; Lacasse, E. Synthesis of Pyran-4-Ones from Isoxazoles. *Tetrahedron Letters* **2002**, *43*
922 (19), 3565–3568. [https://doi.org/10.1016/S0040-4039\(02\)00567-1](https://doi.org/10.1016/S0040-4039(02)00567-1).
- 923 (15) Thummala, Y.; Karunakar, G. V.; Doddi, V. R. DBU-Mediated Synthesis of Aryl Acetylenes or 1-
924 Bromoethynylarenes from Aldehydes. *Adv. Synth. Catal.* **2019**, *361* (3), 611–616.
925 <https://doi.org/10.1002/adsc.201801334>.
- 926 (16) Fang, Y.-Q.; Lifchits, O.; Lautens, M. Horner-Wadsworth-Emmons Modification for Ramirez
927 Gem-Dibromoolefination of Aldehydes and Ketones Using P(Oi-Pr)₃. *Synlett* **2008**, *2008* (3),
928 413–417. <https://doi.org/10.1055/s-2008-1032045>.
- 929 (17) 2-(2,2-DIBROMOETHENYL)-BENZENAMINE. *Org. Synth.* **2009**, *86*, 36–46.
930 <https://doi.org/10.15227/orgsyn.086.0036>.
- 931 (18) Tassano, E.; Alama, A.; Basso, A.; Dondo, G.; Galatini, A.; Riva, R.; Banfi, L. Conjugation of
932 Hydroxytyrosol with Other Natural Phenolic Fragments: From Waste to Antioxidants and
933 Antitumour Compounds: Conjugation of Hydroxytyrosol with Natural Phenolic Fragments. *Eur.*
934 *J. Org. Chem.* **2015**, *2015* (30), 6710–6726. <https://doi.org/10.1002/ejoc.201500931>.
- 935 (19) Valdomir, G.; Padrón, J.; Padrón, J.; Martín, V.; Davyt, D. Oxazole/Thiazole and Triazole Hybrids
936 Based on α -Amino Acids. *Synthesis* **2014**, *46* (18), 2451–2462. <https://doi.org/10.1055/s-0033-1339139>.
- 937 (20) Morri, A. K.; Thummala, Y.; Doddi, V. R. The Dual Role of 1,8-Diazabicyclo[5.4.0]Undec-7-Ene
938 (DBU) in the Synthesis of Terminal Aryl- and Styryl-Acetylenes via Umpolung Reactivity. *Org.*
939 *Lett.* **2015**, *17* (18), 4640–4643. <https://doi.org/10.1021/acs.orglett.5b02398>.
- 940 (21) Miyakoshi, T.; Saito, S.; Kumanotani, J. A NEW SYNTHESIS OF β NITRO CARBONYL COMPOUNDS
941 FROM ALKYL VINYL KETONES WITH SODIUM NITRITE-ACETIC ACID IN TETRAHYDROFURAN.
942 *Chem. Lett.* **1981**, *10* (12), 1677–1678. <https://doi.org/10.1246/cl.1981.1677>.
- 943 (22) Rosini, G.; Ballini, R.; Sorrenti, P. A New Route to 1,4 -Diketones and Its Application to (z)-
944 Jasmone and Dihydrojasmone Synthesis. *Tetrahedron* **1983**, *39* (24), 4127–4132.
945 [https://doi.org/10.1016/S0040-4020\(01\)88632-4](https://doi.org/10.1016/S0040-4020(01)88632-4).
- 946 (23) Mukaiyama, T.; Hoshino, T. The Reactions of Primary Nitroparaffins with Isocyanates¹. *J. Am.*
947 *Chem. Soc.* **1960**, *82* (20), 5339–5342. <https://doi.org/10.1021/ja01505a017>.

- 949 (24) Kulandai Raj, A. S.; Kale, B. S.; Mokar, B. D.; Liu, R.-S. Gold-Catalyzed *N*, *O*-Functionalizations of
950 6-Allenyl-1-Ynes with *N*-Hydroxyanilines To Construct Benzo[*b*]-Azepin-4-One Cores. *Org. Lett.*
951 **2017**, *19* (19), 5340–5343. <https://doi.org/10.1021/acs.orglett.7b02629>.
- 952 (25) Pauli, L.; Tannert, R.; Scheil, R.; Pfaltz, A. Asymmetric Hydrogenation of Furans and Benzofurans
953 with Iridium-Pyridine-Phosphinite Catalysts. *Chem. Eur. J.* **2015**, *21* (4), 1482–1487.
954 <https://doi.org/10.1002/chem.201404903>.
- 955 (26) Rehbein, J.; Leick, S.; Hiersemann, M. Gosteli–Claisen Rearrangement: Substrate Synthesis,
956 Simple Diastereoselectivity, and Kinetic Studies. *J. Org. Chem.* **2009**, *74* (4), 1531–1540.
957 <https://doi.org/10.1021/jo802303m>.
- 958 (27) Persich, P.; Llaveria, J.; Lhermet, R.; de Haro, T.; Stade, R.; Kondoh, A.; Fürstner, A. Increasing
959 the Structural Span of Alkyne Metathesis. *Chem. Eur. J.* **2013**, *19* (39), 13047–13058.
960 <https://doi.org/10.1002/chem.201302320>.
- 961 (28) Zhao, H.-Y.; Wu, F.-S.; Yang, L.; Liang, Y.; Cao, X.-L.; Wang, H.-S.; Pan, Y.-M. Catalyst- and
962 Solvent-Free Approach to 2-Arylated Quinolines *via* [5 + 1] Annulation of 2-Methylquinolines
963 with Diynones. *RSC Adv.* **2018**, *8* (9), 4584–4587. <https://doi.org/10.1039/C7RA12716B>.
- 964 (29) Wang, T.; Shi, S.; Hansmann, M. M.; Rettenmeier, E.; Rudolph, M.; Hashmi, A. S. K. Synthesis of
965 Highly Substituted 3-Formylfurans by a Gold(I)-Catalyzed Oxidation/1,2-Alkynyl
966 Migration/Cyclization Cascade. *Angew. Chem. Int. Ed.* **2014**, *53* (14), 3715–3719.
967 <https://doi.org/10.1002/anie.201310146>.
- 968 (30) Hatano, M.; Sakamoto, T.; Mizuno, T.; Goto, Y.; Ishihara, K. Chiral Supramolecular U-Shaped
969 Catalysts Induce the Multiselective Diels–Alder Reaction of Propargyl Aldehyde. *J. Am. Chem.*
970 *Soc.* **2018**, *140* (47), 16253–16263. <https://doi.org/10.1021/jacs.8b09974>.
- 971 (31) Zhang, S.; An, B.; Yan, J.; Huang, L.; Li, X. The Synthesis and Evaluation of New Benzophenone
972 Derivatives as Tubulin Polymerization Inhibitors. *RSC Adv.* **2016**, *6* (91), 88453–88462.
973 <https://doi.org/10.1039/C6RA16948A>.
- 974 (32) Pilkington, L. I.; Wagoner, J.; Kline, T.; Polyak, S. J.; Barker, D. 1,4-Benzodioxane Lignans: An
975 Efficient, Asymmetric Synthesis of Flavonolignans and Study of Neolignan Cytotoxicity and
976 Antiviral Profiles. *J. Nat. Prod.* **2018**, *81* (12), 2630–2637.
977 <https://doi.org/10.1021/acs.jnatprod.8b00416>.
- 978 (33) Pang, Y.; An, B.; Lou, L.; Zhang, J.; Yan, J.; Huang, L.; Li, X.; Yin, S. Design, Synthesis, and
979 Biological Evaluation of Novel Selenium-Containing *Iso* Combretastatins and Phenstatins as
980 Antitumor Agents. *J. Med. Chem.* **2017**, *60* (17), 7300–7314.
981 <https://doi.org/10.1021/acs.jmedchem.7b00480>.
- 982 (34) Sakata, Y.; Yasui, E.; Mizukami, M.; Nagumo, S. Cascade Reaction Including a Formal [5 + 2]
983 Cycloaddition by Use of Alkyne-Co₂(CO)₆ Complex. *Tetrahedron Letters* **2019**, *60* (11), 755–759.
984 <https://doi.org/10.1016/j.tetlet.2019.01.045>.
- 985 (35) Rosiak, A.; Müller, R. M.; Christoffers, J. Synthesis of 2,3-Dihydrothiopyran-4-Ones from 3-Oxo-
986 1-Pentene-4-Ynes. *Monatsh. Chem.* **2007**, *138* (1), 13–26. [https://doi.org/10.1007/s00706-006-](https://doi.org/10.1007/s00706-006-0571-4)
987 [0571-4](https://doi.org/10.1007/s00706-006-0571-4).
- 988 (36) Tong, W.; Li, Q.-Y.; Xu, Y.-L.; Wang, H.-S.; Chen, Y.-Y.; Pan, Y.-M. An Unexpected Domino
989 Reaction of β -Keto Sulfones with Acetylene Ketones Promoted by Base: Facile Synthesis of 3(2
990 *H*)-Furanones and Sulfonylbenzenes. *Adv. Synth. Catal.* **2017**, *359* (22), 4025–4035.
991 <https://doi.org/10.1002/adsc.201700830>.
- 992 (37) Xu, Y.-L.; Teng, Q.-H.; Tong, W.; Wang, H.-S.; Pan, Y.-M.; Ma, X.-L. Atom-Economic Synthesis of
993 4-Pyrone from Diynones and Water. *Molecules* **2017**, *22* (1), 109.
994 <https://doi.org/10.3390/molecules22010109>.
- 995 (38) Ghandi, M.; Bayat, Y.; Teimuri-Mofrad, R. A NOVEL METHOD FOR THE SYNTHESIS OF FORMYL
996 AND HYDROXYMETHYL DERIVATIVES OF 4 *H*-PYRAN-4-ONE. *Organic Preparations and*
997 *Procedures International* **2002**, *34* (5), 525–530. <https://doi.org/10.1080/00304940209355774>.
- 998 (39) Cao, Y.; Chen, L.; Xi, Y.; Li, Y.; Yan, X. Stimuli-Responsive 2,6-Diarylethene-4H-Pyran-4-One
999 Derivatives: Aggregation Induced Emission Enhancement, Mechanochromism and

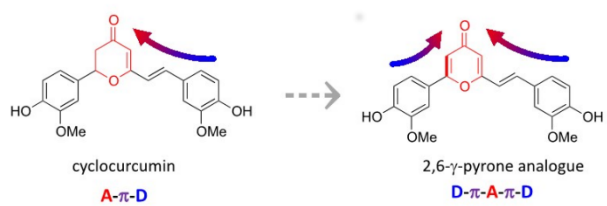
- 1000 Solvatochromism. *Materials Letters* **2018**, *212*, 225–230.
1001 <https://doi.org/10.1016/j.matlet.2017.10.041>.
- 1002 (40) Xia, Y.; Wang, W. Asymmetric Synthesis of Machilin C and Its Analogue. *Chemical Papers* **2010**,
1003 *64* (5). <https://doi.org/10.2478/s11696-010-0040-8>.
- 1004 (41) Faler, C. A.; Joullie, M. M. The Kulinkovich Reaction in the Synthesis of Constrained N,N-Dialkyl
1005 Neurotransmitter Analogues. *ChemInform* **2007**, *38* (38).
1006 <https://doi.org/10.1002/chin.200738058>.
- 1007 (42) Tangdenpaisal, K.; Sualek, S.; Ruchirawat, S.; Ploypradith, P. Factors Affecting Orthogonality in
1008 the Deprotection of 2,4-Di-Protected Aromatic Ethers Employing Solid-Supported Acids.
1009 *Tetrahedron* **2009**, *65* (22), 4316–4325. <https://doi.org/10.1016/j.tet.2009.03.089>.
- 1010 (43) Schmittel, M.; Morbach, G.; Schenk, W. A.; Hagel, M. Synthesis, Thermal Reactivity and
1011 Structure of 1,2-Bis(4-Hydroxy-3-Methoxyphenylethynyl)Benzene. *J Chem Crystallogr* **2005**, *35*
1012 (5), 373–379. <https://doi.org/10.1007/s10870-005-1674-1>.
- 1013 (44) Becke, A. D. Density-functional Thermochemistry. III. The Role of Exact Exchange. *The Journal of*
1014 *Chemical Physics* **1993**, *98* (7), 5648–5652. <https://doi.org/10.1063/1.464913>.
- 1015 (45) Frisch, M. J.; Trucks, G. W.; Schlegel, H. B. **2016**, *Gaussian, Inc.*
- 1016 (46) Yanai, T.; Tew, D. P.; Handy, N. C. A New Hybrid Exchange–Correlation Functional Using the
1017 Coulomb-Attenuating Method (CAM-B3LYP). *Chemical Physics Letters* **2004**, *393* (1–3), 51–57.
1018 <https://doi.org/10.1016/j.cplett.2004.06.011>.
- 1019 (47) Barbatti, M.; Ruckebauer, M.; Plasser, F.; Pittner, J.; Granucci, G.; Persico, M.; Lischka, H.
1020 Newton-X: A Surface-Hopping Program for Nonadiabatic Molecular Dynamics: Newton-X.
1021 *WIREs Comput Mol Sci* **2014**, *4* (1), 26–33. <https://doi.org/10.1002/wcms.1158>.
- 1022 (48) Hehre, W. J.; Ditchfield, R.; Pople, J. A. Self-Consistent Molecular Orbital Methods. XII. Further
1023 Extensions of Gaussian-Type Basis Sets for Use in Molecular Orbital Studies of Organic
1024 Molecules. *The Journal of Chemical Physics* **1972**, *56* (5), 2257–2261.
1025 <https://doi.org/10.1063/1.1677527>.
- 1026 (49) Tomasi, J.; Mennucci, B.; Cammi, R. Quantum Mechanical Continuum Solvation Models. *Chem.*
1027 *Rev.* **2005**, *105* (8), 2999–3094. <https://doi.org/10.1021/cr9904009>.
- 1028 (50) Turan, H. T.; Eken, Y.; Marazzi, M.; Pastore, M.; Aviyente, V.; Monari, A. Assessing One- and
1029 Two-Photon Optical Properties of Boron Containing Arenes. *J. Phys. Chem. C* **2016**, *120* (32),
1030 17916–17926. <https://doi.org/10.1021/acs.jpcc.6b05493>.
- 1031 (51) Marazzi, M.; Gattuso, H.; Monari, A.; Assfeld, X. Steady-State Linear and Non-Linear Optical
1032 Spectroscopy of Organic Chromophores and Bio-Macromolecules. *Front. Chem.* **2018**, *6*, 86.
1033 <https://doi.org/10.3389/fchem.2018.00086>.
- 1034 (52) Gattuso, H.; Dumont, E.; Marazzi, M.; Monari, A. Two-Photon-Absorption DNA Sensitization via
1035 Solvated Electron Production: Unraveling Photochemical Pathways by Molecular Modeling and
1036 Simulation. *Phys. Chem. Chem. Phys.* **2016**, *18* (27), 18598–18606.
1037 <https://doi.org/10.1039/C6CP02592G>.
- 1038 (53) Gattuso, H.; Monari, A.; Marazzi, M. Photophysics of Chlorin E6: From One- and Two-Photon
1039 Absorption to Fluorescence and Phosphorescence. *RSC Adv.* **2017**, *7* (18), 10992–10999.
1040 <https://doi.org/10.1039/C6RA28616J>.
- 1041 (54) Aidas, K.; Angeli, C.; Bak, K. L.; Bakken, V.; Bast, R.; Boman, L.; Christiansen, O.; Cimiraglia, R.;
1042 Coriani, S.; Dahle, P.; Dalskov, E. K.; Ekström, U.; Enevoldsen, T.; Eriksen, J. J.; Ettenhuber, P.;
1043 Fernández, B.; Ferrighi, L.; Fliegl, H.; Frediani, L.; Hald, K.; Halkier, A.; Hättig, C.; Heiberg, H.;
1044 Helgaker, T.; Hennum, A. C.; Hettrema, H.; Hjertenaes, E.; Høst, S.; Høyvik, I.-M.; Iozzi, M. F.;
1045 Jansík, B.; Jensen, H. J. Aa.; Jonsson, D.; Jørgensen, P.; Kauczor, J.; Kirpekar, S.; Kjaergaard, T.;
1046 Klopper, W.; Knecht, S.; Kobayashi, R.; Koch, H.; Kongsted, J.; Krapp, A.; Kristensen, K.; Ligabue,
1047 A.; Lutnaes, O. B.; Melo, J. I.; Mikkelsen, K. V.; Myhre, R. H.; Neiss, C.; Nielsen, C. B.; Norman, P.;
1048 Olsen, J.; Olsen, J. M. H.; Osted, A.; Packer, M. J.; Pawłowski, F.; Pedersen, T. B.; Provasi, P. F.;
1049 Reine, S.; Rinkevicius, Z.; Ruden, T. A.; Ruud, K.; Rybkin, V. V.; Sałek, P.; Samson, C. C. M.; de
1050 Merás, A. S.; Saue, T.; Sauer, S. P. A.; Schimmelpfennig, B.; Sneskov, K.; Steindal, A. H.;
1051 Sylvester-Hvid, K. O.; Taylor, P. R.; Teale, A. M.; Tellgren, E. I.; Tew, D. P.; Thorvaldsen, A. J.;

1052 Thøgersen, L.; Vahtras, O.; Watson, M. A.; Wilson, D. J. D.; Ziolkowski, M.; Ågren, H. The Dalton
1053 Quantum Chemistry Program System: The Dalton Program. *WIREs Comput Mol Sci* **2014**, *4* (3),
1054 269–284. <https://doi.org/10.1002/wcms.1172>.
1055

1056

1057

1058



1059

1060